Modelling Axial Turbomachinery for Compressed Air Energy Storage

by

Jorge Gonzalez Gonzalez

A thesis
presented to the University of Waterloo
in fulfillment of the
thesis requirement for the degree of
Master of Applied Science
in
Mechanical and Mechatronics Engineering

Waterloo, Ontario, Canada, 2018

AUTHOR'S DECLARATION

I hereby declare that I am the sole author of this thesis. This is a true copy of the thesis, including any required final revisions, as accepted by my examiners.

I understand that my thesis may be made electronically available to the public.

Abstract

Climate change and negative environmental effects from a human's life style have ignited the search for grid-scale electricity production from renewable energy sources. Significant advances with respect to renewable energy conversion into electricity has been achieved in recent years. However, their integration with the electrical grid is still an unsolved problem because the natural intermittency associated with them. Grid-scale energy storage can be the solution to the intermittency problem; of all the types or storage, compressed air energy storage (CAES) is one of the most promising potential solutions to effectively integrate renewable energies to the grid.

CAES consists in compressing air during times when the electricity production is larger than the demand. This compressed air is stored in a huge reservoir; it is then used during peak demand times to run gas turbines which are connected to power generators. Literature about steady state CAES is widely available; topics such as system efficiency, fuel free CAES, and reservoir sizing being arguably the most commonly published. However, there are very few works about dynamic state of a CAES system; and there are next to no publications regarding the transient modelling of the turbomachinery for CAES.

This thesis develops two independent dynamic models of axial turbomachines for CAES systems; one for a compressor and one for a turbine. These models should be able to represent the behavior of the machines, as well as easily connect with the rest of the components of the system. For these reasons, the models are developed in the SIMULINK® environment, which is a tool commonly used for electrical modelling. The models use the time domain, and are based on compressor and turbine performance maps, which make them representative, and let them require a short simulation time.

The objective of the simulations is to see how the models behave with regards to power inefficiency, part-load operation; and the effects on the complete operation caused by the system inertias. The models can replicate the operation of any axial turbomachine provided the respective map, and can be also used with centrifugal compressors. Upon running the simulations, a round trip efficiency of 55% was obtained. Furthermore, it takes 296 seconds to increase the pressure of a cavern of 3000 m^3 from 422.18 Kpa to 747.4 Kpa. The simulated turbine of 167 MW and design speed of 17000 rpm, with a nominal mass flow rate of 400 kg/s, will take 778 seconds to reach its nominal speed.

Acknowledgements

I want to thank my supervisor Professor Roydon A. Fraser for his infinite help and support.

I want to thank also the Science and Technology Counsel of Mexico, CONACYT, who supported me financially for 24 months.

Last but not least, I want to thank my friends Sid, Ivan, Mehrdad, Erick, and Ehsan, for their help and support.

Dedication

A mi mamá, mi luz, mi guía, sin ti no hubiera podido lograrlo. Quiero que sepas que este éxito es más tuyo que mío. Siempre que me caigo me levantas, y siempre estás ahí. Te quiero con todas mis fuerzas.

A mi papá, te extraño mucho, esto es para ti.

To my mom, my light, my guide, without you I wouldn't have achieved it. I want you to know that this success is more yours than mine. Every time I fall down you help me get up, you are always there. I love you with all my strength.

To my dad, I miss you so much, this is for you.

Table of Contents

List of Figures

List of Tables

Nomenclature

a	Speed of Sound
C_p	Specific Heat at Constant Pressure
d	Diameter
F	Friction Factor, Force
G_c	Compressor Torque
G_l	Load Torque
G_t	Turbine Torque
h	Specific Enthalpy
H	Total Enthalpy
i	Incidence
I	Moment of Inertia
k	Specific Heats Ratio, Square Fit Coefficient
m	Mass
$\dot{m}$	Mass Flow Rate
P	Power
p	Pressure
P_r	Pressure Ratio
$\dot{Q}$	Heat Transfer Rate
R	Gas Constant
r	Radius
T	Torque, Temperature
t	Time
U	Angular Speed
u	Axial Velocity
V	Velocity, Volume
$\dot{W}_s$	Shaft Power
α	Angle
η	Efficiency
ρ	Density
Ψ	Pressure Coefficient
ω	Angular Speed

Φ	Flow Coefficient
i'_{dr}	D Axis Rotor Current
i_{ds}	D Axis Stator Current
i'_{qr}	Q Axis Rotor Current
i_{qs}	Q Axis Stator Current
L'_{lr}	Rotor Leakage Inductance
L_{ls}	Stator Leakage Inductance
L_m	Magnetizing Inductance
L_m	Magnetizing Inductance
L'_r	Total Rotor Inductance
L_s	Total Stator Inductance
L_s	Total Stator Inductance
p	Number of Pole Pairs
R'_r	Rotor Resistance
R_s	Stator Resistance
T_e	Electromagnetic Torque
T_m	Shaft Mechanical Torque
V'_{dr}	D Axis Rotor Voltage
V_{ds}	D Axis Stator Voltage
V'_{qr}	Q Axis Rotor Voltage
V_{qs}	Q Axis Stator Voltage
ϕ'_{dr}	D Axis Rotor Flux
ϕ_{ds}	D Axis Stator Flux
ϕ'_{qr}	Q Axis Rotor Flux
ϕ_{qs}	Q Axis Stator Flux
ω_m	Rotor Angular Velocity
ω_r	Electrical Angular Velocity

Suffixes

1	Inlet, Ambient
2	Outlet, After Compression
3	Before Expansion
4	After Expansion
isen	Isentropic Process
θ	Tangential

Chapter 1
Introduction

The way humans have been utilizing natural resources the last two hundred years is unsustainable and is heading towards bringing forth a global energy crisis [1]. In recent years, there has been an added emphasis on developing clean energy technology around the world [2]. One of the areas that has received attention is electricity production and distribution. Today, manufacturers of wind turbines and other similar expertise have developed technologies that are both efficient and powerful; however, a gap exists that must be bridged when it comes to the implementation of these technologies in an urban grid. This problem lies with intermittency of energy supply to the grid from renewable energy sources. For example, electricity production from wind turbines depends on the availability of the right wind conditions to run the generators. When these conditions are not met, there is not sufficient electricity production. Since this can happen at any time on any day; if an urban power grid were to rely solely on wind turbines for its energy supply, it would be too chaotic and unreliable for the supplier, as well as the consumers. Therefore, electricity production systems based on renewable energies need to interface with a grid-scale storage system before the connection to a grid. Pumped hydro is the most commonly used method of grid-scale energy storage; however, the construction of new pumped hydro dams comes with significant consequences to the environment and elevated costs. Furthermore, their operation affects fauna present in the area [3].

Compressed air energy storage (CAES) is one of the most promising potential solutions to effectively integrate renewable energies to the grid [4]. In its core configuration, CAES operates by compressing air using excess energy from the grid to then store it in an underground reservoir. When required by the grid, the air is reheated and expanded in a turbine which is connected to a power generator to produce electricity, as seen on Figure 1.

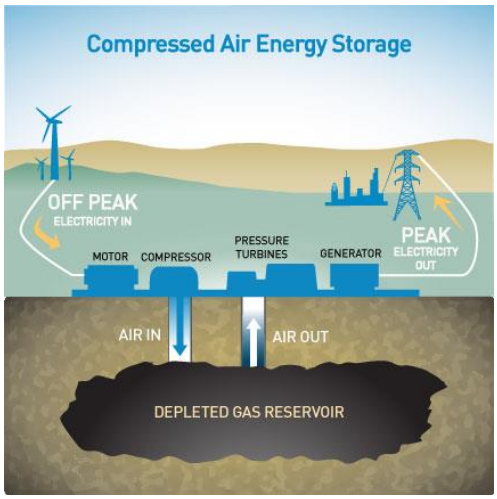

Figure 1 Generic Compressed Air Energy Storage Diagram [5]

There are currently two fully functional CAES plants that exist in the world. One in Huntorf Germany, and the other in Alabama U.S. Both plants work using the aforementioned principle: using excess energy from the grid to store ambient air in underground salt reservoirs, and then using combustion chambers and turbines to run generators [6]. Another configuration of a CAES system could be to use wind turbines or solar energy to feed the system instead of excess energy from the grid [7]. In this way, the intermittency of the renewable source could be regulated using a reservoir capable of containing an amount of compressed air large enough to produce several hours of grid-scale power.

1.1 Motivation

In literature, there are many publications about CAES that touch a wide range of topics The current CAES literature primarily focus on the following: (1) low-fidelity thermodynamic modelling of efficiency for gas turbine-based CAES systems [8]–[10] with some validated against the existing Huntorf CAES system in Germany [11], (2) cavern heat transfer validated against the Huntorf CAES system[12]–[15], (3) low-fidelity thermodynamic modelling of efficiency for adiabatic [16]–[23] or isothermal CAES systems [24], (4) adiabatic or isothermal CAES heat storage and heat transfer options [25]–[29], and (5) low-fidelity strategic integration of CAES systems into an energy network that includes, for example, wind turbines [7], [30]–[32]. Lacking in the literature are studies into the application of CAES to specific electricity grids each of which have their own consideration in terms of CAES locating, grid infrastructure, and grid management. Also lacking are high-fidelity CAES

models capable of capturing system transients such as variable turbine speed-load efficiency and rotary machinery inertia, and of capturing detailed cavern dynamics and heat transfer.

1.2 Objective

The objective of this thesis is to create models of the turbomachinery parts of the overall CAES system. These models should be able to represent simulate the behavior of the machines, as well as easily connect with the rest of the components of the system. This means that the models must be flexible enough for customization, should be able to be used with an external control strategy, and run the simulation relatively fast. Due to these reasons, this work contains two models of axial turbomachinery, one of the axial compressor, and one of the turbine.

1.3 Thesis Outline

This thesis is divided into six different chapters.

Chapter 1 provides motivation for energy storage and gives an overview of CAES.

Chapter 2 contains a review of the published literature of turbomachinery models, and techniques used in them for data interpretation and collection.

Chapter 3 explains what a turbomachine is, their working principles, main components, and types of machines. Chapter 3 also points out specific thermodynamics and fluid mechanics phenomena that are closely related to the topic, as well as how these are integrated in turbomachinery maps, which are then used in models.

Chapter 4 details how the models are built for simulation. Starting with the thermodynamic aspects of the compressor followed by how to connect them with the rotational motion of the machine. After that, it explains how the data is read from the compressor maps and details the solving sequence for that model. The second part of Chapter 4 contains the turbine model; it keeps the same structure as the compressor section. Starting with the thermodynamic aspects of the model, followed by the connection of the model with the rotational motion. After that, the solving sequence for this model is presented.

Chapter 5 shows the results obtained from the simulations. The first part shows the compressor's simulation results and the second part shows the turbine's simulation results. Both sections explain how the results obtained match the expected performance, and concludes explaining why they could not be compared with real data.

Chapter 6 contains the main conclusions found after this work, and outlines recommendations for future work.

Chapter 2
Literature Review

This chapter discusses the various CAES and turbomachinery models published in literature. Models capturing transient effects in the system are important to enable future CAES systems to be designed to deliver ancillary services in addition to arbitrage services; and for developing grid-integration system control strategies. Parameters such as cavern dynamics and heat transfer will affect system capacity, cycle frequency, and life. This work focusses on increasing the fidelity of the axial compressor and turbine models used in CAES systems, and therefore, this literature review starts by considering existing non-CAES models of compressors and turbines.

2.1 Gas Turbine Engine Models

Gas turbine engine dynamic models can be classified into two distinct types, models based on control theory and use the s-domain, and models executed on the time domain. Both types are reviewed in the next two sections.

2.1.1 Models based on Control Theory

In 1983, while working for the turbine division at General Electric, W. I. Rowen [33] published the first model capable of simulating the behavior of multiple GE single-shaft gas turbines for power generation. The Rowen model became the foundation for all other frequency domain base models since published; the model uses transfer functions and linear equations to simulate all the components of a particular gas turbine engine. Figure 2 below shows part of Rowen's model.

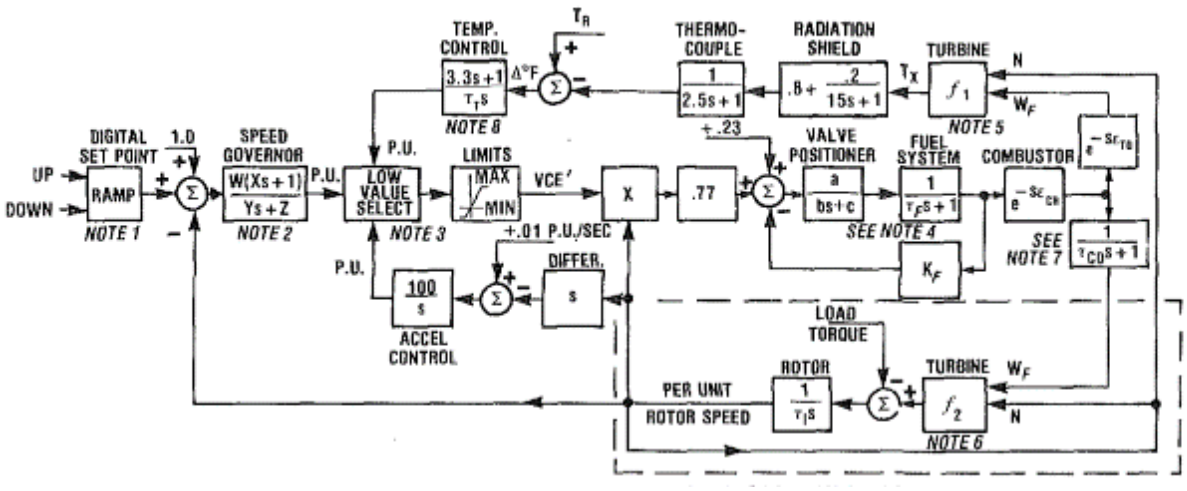

Figure 2 Fragment of Rowen's Model, from [33]

In the Rowen model, values for parameters such as gains, time constants, and other coefficients were obtained from tests and field experience; this data can be found in the article. The simulations done with this model represent with good accuracy the group of gas turbines it aims to study. However, the article does not mention how the model would change if a different turbine is attempted to be simulated with it. Furthermore, Mantzaris and Vournas [34] presented a model similar to Rowen's. In their model they acquired the data needed to perform the simulation from three different sources. Their results show that the time constant values used in the model affect the transient performance results drastically; thus, confirming that frequency domain models are suitable to be used when attempting to study a specific gas turbine or a specific group of gas turbines with accompanying data. Shalan et al. [35] further studied the Rowen model with the use of a lab-turbine engine different from the ones referenced in Rowen's model; the goal was to find the values for the simulation parameters needed to replicate the lab-turbine using Rowen's model. They were able to accurately simulate the turbine, and in order to accomplish this, they used the mathematical calculations published by Tavakoli [36], to estimate the parameters used by Rowen in the mechanical power block section of the model. This is illustrated below in Figure 3 and Figure 4. These constants can be calibrated until they fit the selected engine.

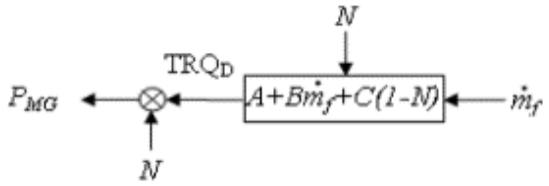

Figure 3 Output Mechanical Power Block of Shalan's Model, from [35]

$$A = \frac{\dot{m}_n \cdot T_1}{P_{Gn}} \left\{ C_{ph} \cdot \eta_t \cdot \left(1 - \frac{1}{x_h}\right) - \frac{x_c - 1}{\eta_c} \times \left[C_{pc} - C_{ph} \cdot \eta_t \cdot \left(1 - \frac{1}{x_h}\right) \right] \right\}$$

$$B = \frac{\eta_{comb} \cdot \eta_t \cdot H \cdot \dot{m}_{fn}}{P_{Gn}} \left(1 - \frac{1}{x_h}\right)$$

Figure 4 Mathematical Calculations for Rowen's Parameters Estimation, from [36]

The Institute of Electrical and Electronic Engineers (IEEE) published a model of a combined cycle power plant using the frequency domain [37]. The purpose of the publication is to have a generic model capable of simulating these type of plants, and to standardize the modelling of this type of plants around the world. An example can be seen below in Figure 5.

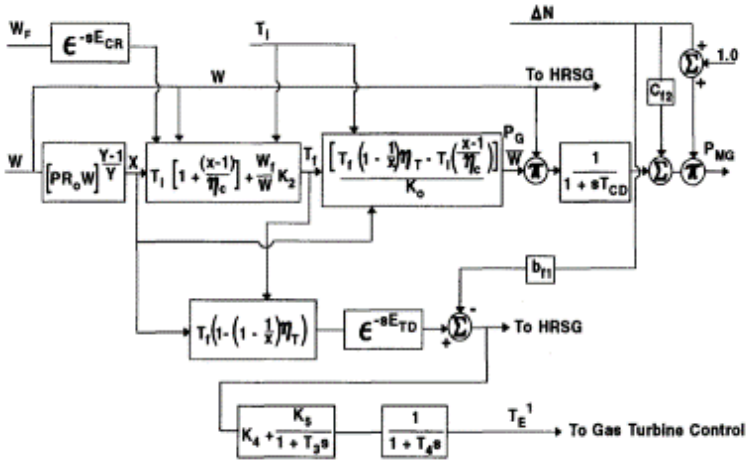

Figure 5 Gas Turbine Blocks of the IEEE Model, from [37]

The IEEE model assumes a fixed compressor ratio, which according to Yee et al., fits only systems that simulate constant speed or steady state operation [38]. Furthermore, although the IEEE model fits the general operation of a gas turbine plant, it does not simulate the start up of the engine. Although all models mentioned in this section gave satisfactory results, they are limited because they represent, with a certain degree of accuracy, only a specific series of turbines and an specific range of operation, which does not include all the phases of the turbomachinery operation. An important point to highlight, which will make more sense at the end of this chapter, is that when using frequency domain models, various constants and parameters need to be derived and then validated against experimentally obtained data, specifically for the turbine of interest to be modelled; otherwise, the turbine behavior achieved in the simulation would be considerably different than the physical engine to be modeled [38].

2.1.2 Time Domain Models

Models on the time domain, use the differential versions of the momentum, mass, and energy conservation equations. These are seen below in equations (1),(2),(3), as well as the rotational motion equation (4) , from [39].

$$V\frac{d(\rho u)_{i+1}}{dt} = -(\dot{m}_{i+1}u_{i+1} - \dot{m}_i u_i + p_{i+1}A_{i+1} - p_i A_i) + F \tag{1}$$

$$V\frac{d(\rho_{i+1})}{dt} = -\dot{m}_{i+1} + \dot{m}_i \tag{2}$$

$$V\frac{d(\rho H - p)_{i+1}}{dt} = -(\dot{m}_{i+1}H_{i+1} - \dot{m}_i H_i) + \dot{Q} - \dot{W}_s \tag{3}$$

$$I\frac{d\omega}{dt} = G_t + G_c + G_l \tag{4}$$

Where is V the volume, ρ the density, $\dot{m}$ the mass flow rate, u the axial velocity, p the static pressure, A the area, F the force, H total enthalpy, $\dot{Q}$ the heat transfer rate, $\dot{W}_s$ the shaft power, G_t the turbine torque, G_c the compressor torque, and G_l the load torque. These equations need some data from a

reliable source in order to solve them; and because of this, these types of models can be also classified into two distinct categories: those who use compressor and turbine maps, and those who obtain the required data directly from the manufacturer. The models that use maps can use distinct approaches to retrieve data; section 2.2 of this thesis will discuss this further. A considerable number of models using the time domain are available in literature. Kim et al. [40] modeled a single spool turbojet engine using turbomachinery maps and beta lines. Further discussion on beta lines and their application are present in section 2.2 of this thesis. With the maps' data, they produced lookup tables and used linear interpolation to estimate the value of the required parameters. For the turbine map, a single speed line assumption was made. The results show that this assumption does not model the system very accurately at low speeds. However, at higher speeds, the results are representative. Ismail and Bhinder [41] created a computer program that simulates an aircraft engine; their work also uses compressor maps to build lookup tables, and Lagrangian interpolation for inter-value estimations. Their results were never compared to real data, but according to the authors, the trend shown on the diagrams fits the predicted results correctly. Al-Hamdan and Ebaid [42], modeled a gas turbine for power generation, using beta lines, three dimensional look-up tables, and linear interpolation. Their work focuses on predicting the running line of a turbine engine by matching the compressor and turbine mass flow rates and speeds; this is done by superimposing both maps. The authors did not compare their results to test data, and their running line contribution is specific to a certain compressor and turbine model. Bettocchi and Fabbri [43] developed a model for diagnostics and measurement, as well as control sensors of an industrial gas turbine. Their model divides the turbine engine into the following blocks: compressor, combustor, and turbine; and assumes that each block is connected to a constant section duct. Bettochi's and Fabbri's model uses compressor maps, but no interpolation method is discussed. The simulation results were satisfactorily compared to measurements taken from a single-shaft gas turbine in operation. Crosa et al. [44] developed a model that splits the compressor map into different sections according to their pressure ratio. The model uses performance maps and linear interpolation; their results could not be compared to real data, but they were satisfactorily compared to the results given by an older FORTRAN 77 model published by the same authors; which was previously compared satisfactorily to a test engine. Camporeale et al.[45] developed a real-time model of a gas turbine for power generation; the model considers compressor and turbine as volume-less objects, and adds a plenum after each turbomachine for mass calculations. The model uses bilinear interpolation to estimate data from the maps; their results were compared well to previously published data.

Other publications have modeled gas turbine engines without using performance maps [39], [46], [47]. Instead, these articles have used stage characteristic curves. Stages characteristics represent the relationship between the flow coefficient, pressure coefficient, and efficiency, as seen in Figure 6 and Figure 7. From the curves, data is retrieved and used to solve a system of differential equations, by an iterative procedure.

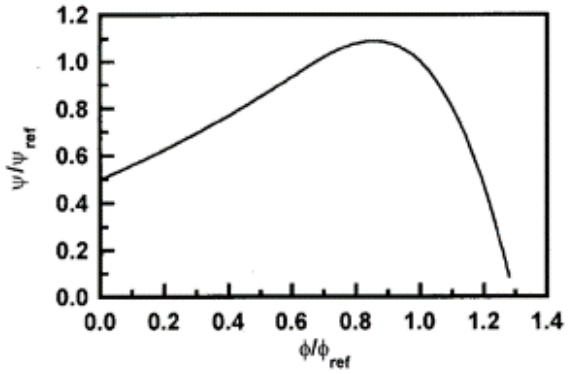

Figure 6 Pressure Coefficient Stage Characteristic Curve Example, from [47]

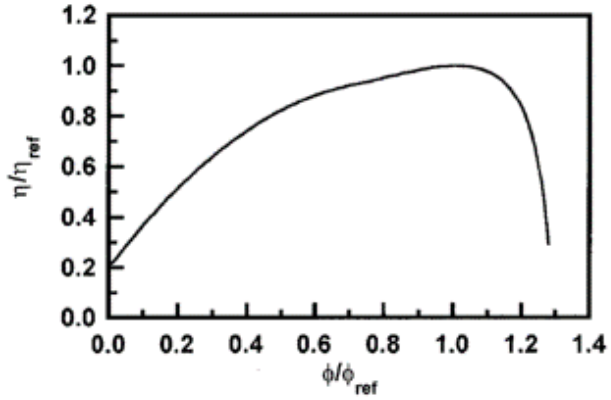

Figure 7 Isentropic Efficiency Stage Characteristic Curve Example, from [47]

The stage curves used in these kinds of models also needs to be obtained from the manufacturers or empirical test. All the gas turbine engine models obtained by the author require empirical data, this is the major limitation of turbomachinery modeling. However, the methods used in them can be reused to model another specific model of the machine, only the source data needs to be changed. The different ways that authors read data from turbomachinery maps is arguably the most significant

difference between the time domain models; for this reason, section 2.2 has been added to this work to further understand these approaches.

2.2 Reading Data from Operation Maps

Compressor maps are used abundantly for the simulation of turbomachinery. Further discussion of what they contain and why all of them have almost the same shape is shown in section 3.3 of Chapter 3. In this chapter, the focus is on how the data is extracted from the compressor maps.

Kurzke [48] created the beta lines method. This is one of the most commonly used approaches in turbomachinery literature. Beta lines, as seen in Figure 8 and Figure 9, are equally spaced parabolic lines or equally spaced straight lines parallel to the surge line that cover the complete range of operation of the compressor map. They eventually work as one of the axis to be used in look-up tables [49]. Angular speed and pressure ratio are given as inputs; then, a beta value is guessed and corrected until it matches both parameters. The correct beta value is then used as one of the axis of an interpolation table to get mass flow rate or efficiency. A graphical example of this is given below in Figure 10.

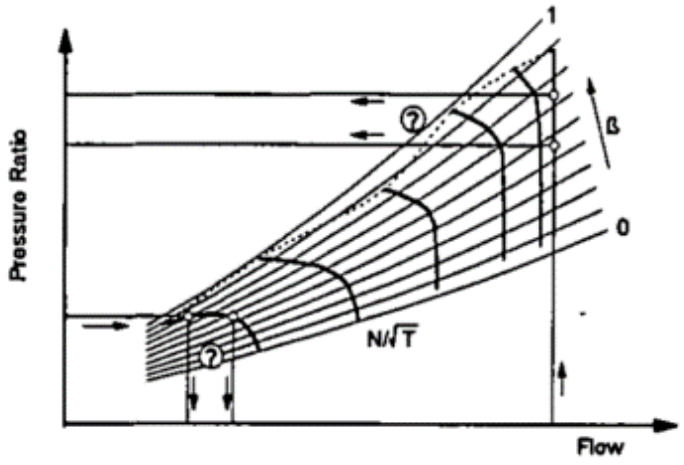

Figure 8 Parabolic Beta Lines on Compressor Map Example, from [48]

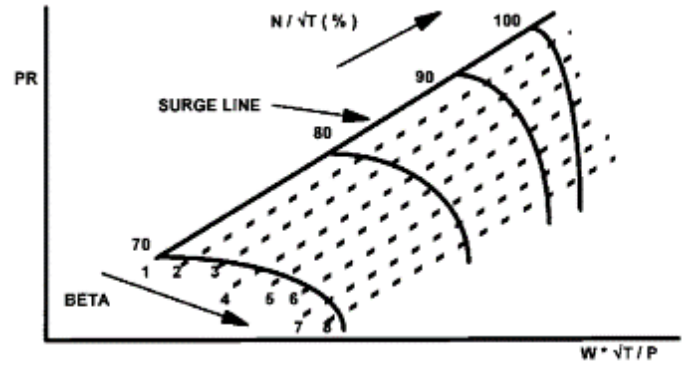

Figure 9 Straight Beta Lines on Compressor Map Example, from [49]

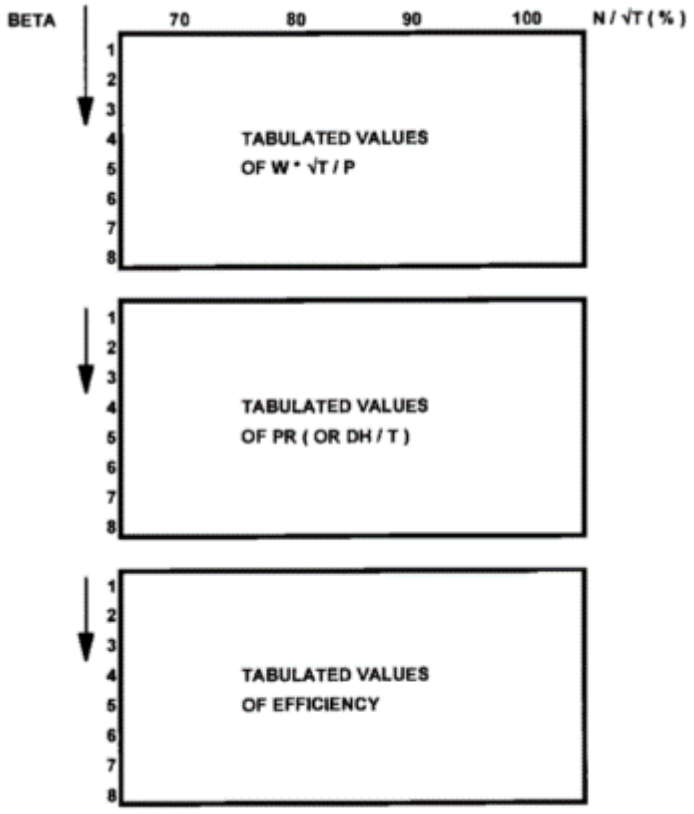

Figure 10 Example of Look-Up Tables with Beta Lines from [49]

Another way to retrieve data from compressor maps is by using artificial neural networks. Some articles [50], [51] among others, studied the use of neural networks to read and extrapolate data of compressor and turbine maps. Moraal and Kolmanovsky [51] found that using a neural network

involves using one hidden layer, n_n neurons, n_u inputs and n_y outputs. In order to accurately use a network to read a compressor map, the pressure ratio should be the unknown variable. When the mass flow rate becomes an additional unknown, the neural networks method cannot obtain an accurate estimation [51]. For turbine maps, using artificial neural networks would mean the addition of artificial mapping points to be able to estimate the performance at very low speeds, thus making it not a suitable method for modelling turbomachines [51]. Jensen et. al. published a different method for capturing the data of a compressor map [52]. It uses the least square fitting technique on experimental data, to find the coefficients *k* in equations (5) and (6). Then with the obtained data it attempts to solve either equation (7) or (8) which are the representations of mass flow rate and pressure ratio respectively.

$$\Psi = \frac{k_1 + k_2\Phi}{k_3 - \Phi} \tag{5}$$

$$\Phi = \frac{k_3\Psi - k_1}{k_2 + \Psi} \tag{6}$$

$$\dot{m} = \Phi\rho_a \frac{\pi}{4} d_c^2 U_c \tag{7}$$

$$\frac{p_{out}}{p_{in}} = \left(\frac{\frac{1}{2}U_c^2\Psi}{C_p T_a} + 1\right)^{\frac{k}{k-1}} \tag{8}$$

In the last four equations, Ψ is the pressure coefficient, Φ the flow coefficient, $\dot{m}$ the mass flow rate, U_c the angular speed, d_c the effective diameter of the compressor, T_a the air temperature, *k* the least square fit coefficients, C_p specific heat at constant pressure, and p the pressure.

Orkisz and Stawarz [53], published a method that uses two variable functions to capture data from compressor maps. This method uses a concept similar to the beta lines called Z lines, and adds some equations for additional detail.

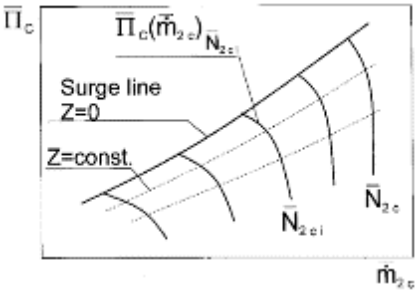

Figure 11 Compressor Map with Z Lines Example, from [53]

This method assumes the mass flow rate, $\bar{\dot{m}}_{2c}$, and the isentropic efficiency, η_c, as second-degree polynomials, and uses the square fitting method to find the coefficients A and B as seen on equations (9) and (10).

$$\bar{\dot{m}}_{2c} = A_0 + A_1\bar{N}_{2c}^2 + A_3\bar{N}_{2c}Z + A_4Z + A_5Z^2 \quad (9)$$

$$\eta_c = B_0 + B_1\bar{N}_{2c} + B_2\bar{N}_{2c}^2 + B_3\bar{N}_{2c}Z + B_4Z + B_5Z^2 \quad (10)$$

After this is done, and iterative solution is then run to get the estimated final values, as seen in Figure 12.

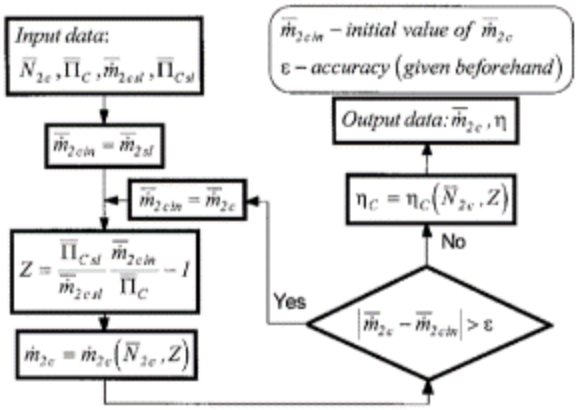

Figure 12 Iterative Solution of Z Lines Method, from [53]**.**

All the available literature on gas turbine engine models require the compressor and turbine to be interconnected by a common shaft. This is an essential part of the solving method; none of these models can predict the performance of a compressor if a turbine is not connected to it, because it obtains data from one machine to feed the other. For the purposes of CAES modelling, turbines and compressors require to be modelled completely independent of each other. Thus, the gas turbine engine methods need to be adapted and modified to accurately represent CAES operation.

The objective of this work is to make dynamic models of an axial turbine and an axial compressor, that can be capable of representing the behaviour of these machines. These models are going to be used for CAES simulations. After reviewing what is available the literature, the author decided that the best approach for this project is to model the machines using maps. Also, beta lines are chosen as the method for reading data because of the accuracy, and level of complexity that it requires

compared to the others. The main differences between this work and previous published ones, is that the compressor and turbine models are entirely independent of each other. Furthermore, the models contain the compressor driver and the turbine load, who are commonly assumed without considering time transients. To help the reader to comprehend these machines, the following chapter contains a detailed explanation of what occurs in them.

Chapter 3
Turbomachinery Concepts and Operation

The purpose of this chapter is to provide to the reader the background theory of the models developed on Chapter 4. First, it contains the general concept of what a turbomachine does; then, it shows some physical conditions that happen during operation which are key to know the limitations and constrains of these machines. Subsections 3.2.1 to 3.2.1, explain these physical phenomena and constrains. Section 3.3 wraps up all these concepts and explains how they contribute to the models in Chapter 4.

3.1 Parts of Axial Turbomachinery

An axial turbomachine has several rows of fixed and moving blades, called stators and rotors respectively. A stator is a row of fixed blades, they guide the fluid in a specific direction and can also function as nozzles or diffusers. A rotor is a row of moving blades attached either directly to the shaft or to a disk connected to the shaft; they either spin the fluid, as in a compressor, or are spun by the fluid as in a turbine. Rotor and stator are arranged one behind the other in a consecutive pattern, as seen in Figure 13. A group of one stator and one rotor is called a stage; this term will be widely used in this work.

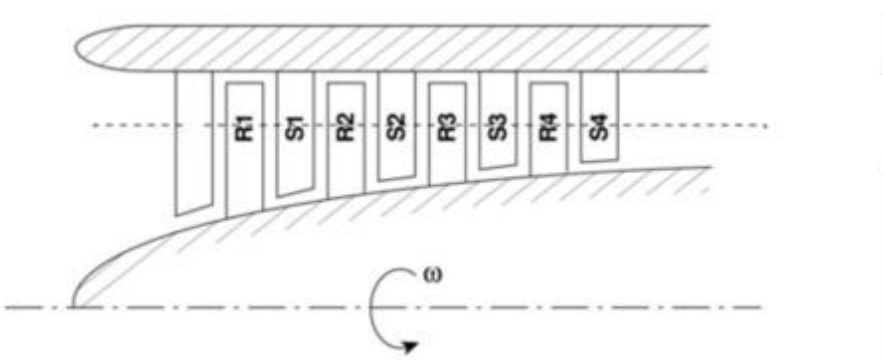

Figure 13 Typical Axial Compressor Configuration, adapted from [54]

3.2 Turbomachinery Operation

In an axial compressor, rotor blades increase the absolute velocity of the fluid and its static temperature; therefore, its absolute temperature increases, and this creates an increase in enthalpy. Within the rotor blade rows, the relative velocity of the fluid decreases, thus producing an increment

in static pressure. The stator vanes diffuse the fluid, decreasing its speed and further increasing its static pressure. This is how a compressor completes its goal of increasing the fluid's static pressure.

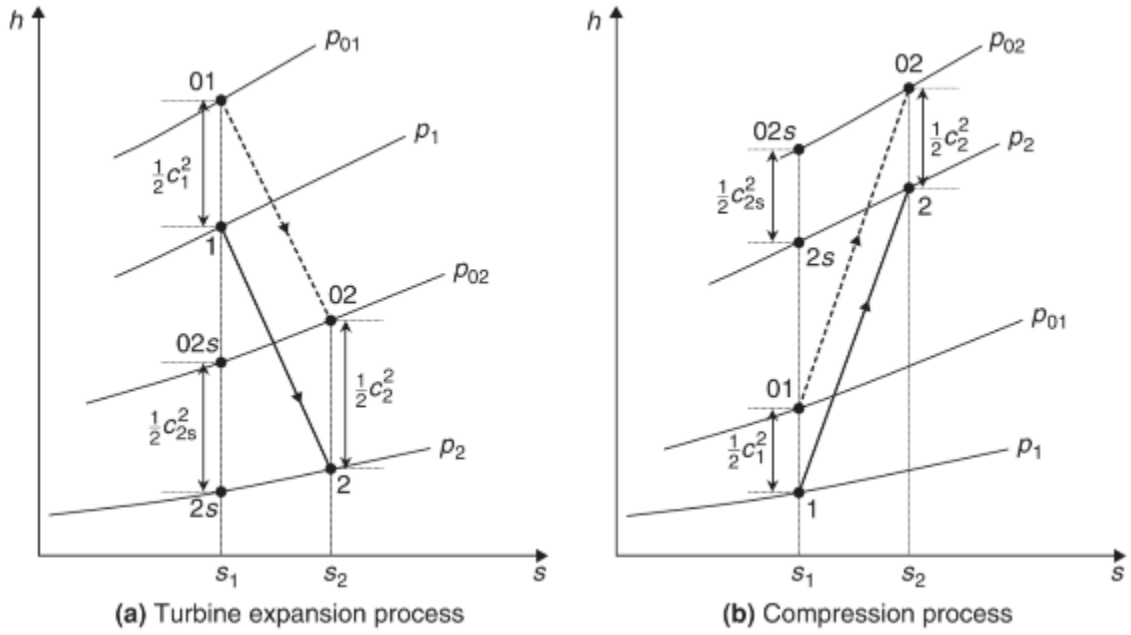

Figure 14 Turbine and Compressor h-s diagrams, from [55]

In a turbine, stator vanes work as nozzles, increasing the absolute velocity of the fluid while decreasing its static pressure and keeping the total temperature constant; then the fluid goes through the rotor, which changes the whirl velocity, reducing the total temperature and total pressure. This is how a turbine converts the pressure energy of the fluid into kinetic energy, which is then retrieved as rotational motion. It is important to understand that the power input or output, according to each machine type, is achieved entirely by the change in angular momentum of the fluid, as seen in equation (11) [55]–[58]; Also, that the energy exchange occurs in the rotor since it is the only moving part of the machine [59].

$$P = T\omega = \dot{m}\omega(V_{2\theta}r_2 - V_{1\theta}r_1) \tag{11}$$

Where T is torque, ω is the angular velocity, V_θ is the tangential velocity, r the mean blade radius and the suffixes 2 and 1 means output and input to the rotor blades respectively.

3.2.1 Speed of Sound and Mach number

Speed of sound is a key parameter in the study of turbomachinery, since at different ranges for the value of the speed of sound, the flow can behave completely different. The speed of sound of a fluid, as defined by White is

> *"The rate of propagation of a pressure pulse of infinitesimal strength through a still fluid."* [60]

The speed of sound is a thermodynamic property, equation (12), from [60], defines it for an ideal gas

$$Speed\ of\ Sound = a = \left(\frac{kp}{\rho}\right)^{\frac{1}{2}} = (kRT)^{\frac{1}{2}} \tag{12}$$

Where k is specific heats ratio, p the pressure, ρ the density, and R the gas constant. Equation (12) shows that the speed of sound will increase as the square root of the absolute temperature. The relation between the speed of sound of a fluid and the velocity of that flow is called Mach number. Equation (13), from [60], defines the Mach number.

$$Mach\ number = \frac{Fluid\ Velocity}{a} \tag{13}$$

For the scope of this work, Mach numbers can be classified into three distinct types: subsonic, which are all the Mach numbers whose value is smaller than 1; supersonic, which are all the ones greater than 1; and sonic, which are the ones equal to 1. When a flowing fluid experiments an area change, e.g. a fluid passing through a nozzle, its Mach number will dictate what physical event occurs to it. Section 3.2.2 details this behavior.

3.2.2 Area Change and Working Fluid

From here on, for simplification, a decrease of available area where a fluid passes is going to be referred as a nozzle, also an increase of the flowing area is going to be referred as diffuser. When a subsonic fluid passes through a nozzle, its pressure and enthalpy decrease while its speed increases. A nozzle does not produce work. It is adiabatic since it's length and the high speed of the working fluid, do not allow heat to be exchanged to the exterior; it is not isentropic since there are friction losses in it [61].

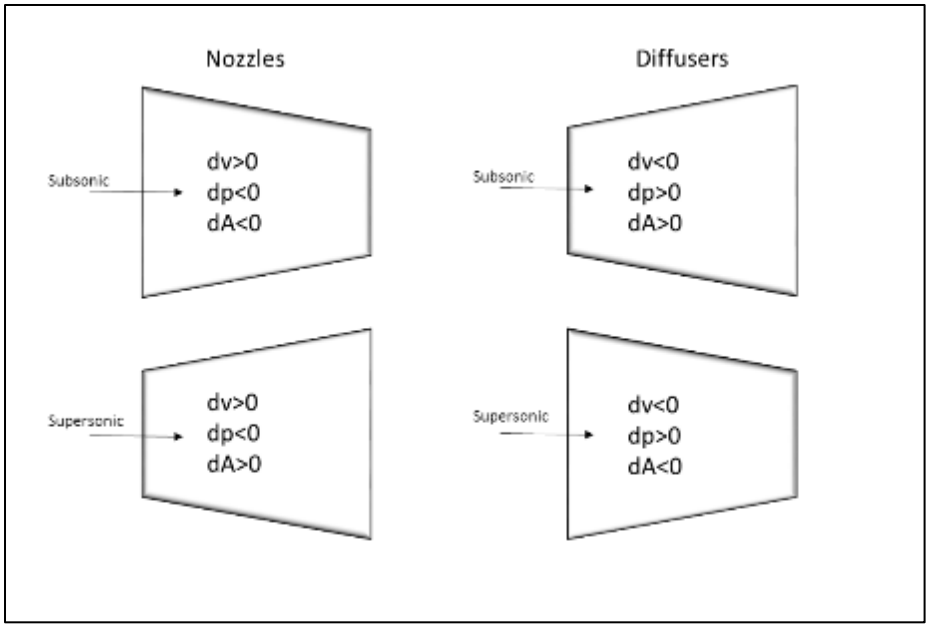

Figure 15 Nozzles and Diffusers Phenomena

When a fluid passes through a nozzle at a supersonic speed, it experiences a pressure increase and a speed reduction, therefore it behaves as a diffuser, see Figure 15. A diffuser is like a nozzle but with an inverted shape. The goal of the diffuser is to increase the pressure of the subsonic fluid while reducing its speed, thus increasing the enthalpy. Like the nozzle, when a fluid with supersonic speed passes through a diffuser, it experiences the inverse phenomenon to subsonic flow; therefore, a supersonic fluid that passes through a diffuser experiences a decrease of pressure and an increase of speed. Area reductions are present in turbomachines, especially in turbines which is a key reason of how this machine works.

3.2.3 Boundary Layer Separation

When a laminar flow is in contact with a surface, its homogeneous speed distribution is changed into a non-uniform shape, because there is a no-slip condition at the wall that retards the flow and produces diffusion [60], as seen in Figure 16. The section of the flow where the speed is not the free flow speed is known as the boundary layer.

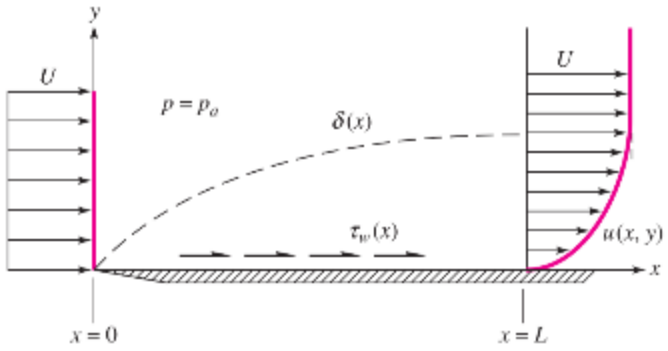

Figure 16 Boundary Layer Shape, from [60]

A smooth boundary layer like the one at the right side of Figure 16, will not produce any considerable issue in a turbomachine. However, according to the pressure gradient present in the duct, the boundary layer might behave in an different way which could cause discrepancies. A favorable pressure gradient, where the flow goes from a high pressure to a lower pressure, as illustrated in Figure 17 A, will ensure the boundary layer to have a smooth shape. With only one curve with no inflection point, and have the minimum losses possible. A zero-pressure gradient, will work as a favorable pressure gradient, such that the difference being that the point of inflection will be exactly where the fluid touches the surface, as in Figure 17 B. A weak adverse gradient, as seen in Figure 17 C, where the flow goes from a lower to a higher pressure, will lose the previously mentioned shape and will acquire a curved shape with an inflection point not at the bottom but higher; it will have two different curves due to the inflection point, and it will not present backflow. A moderate adverse pressure gradient, as in Figure 17 D, will create a critical condition where the wall shear stress is equal to zero, this will be the last moment before backflow occurs, which is not good for the machine's operation. A strong adverse pressure gradient will create backflow, increased losses, and part of the pressure rise will be lost [56].

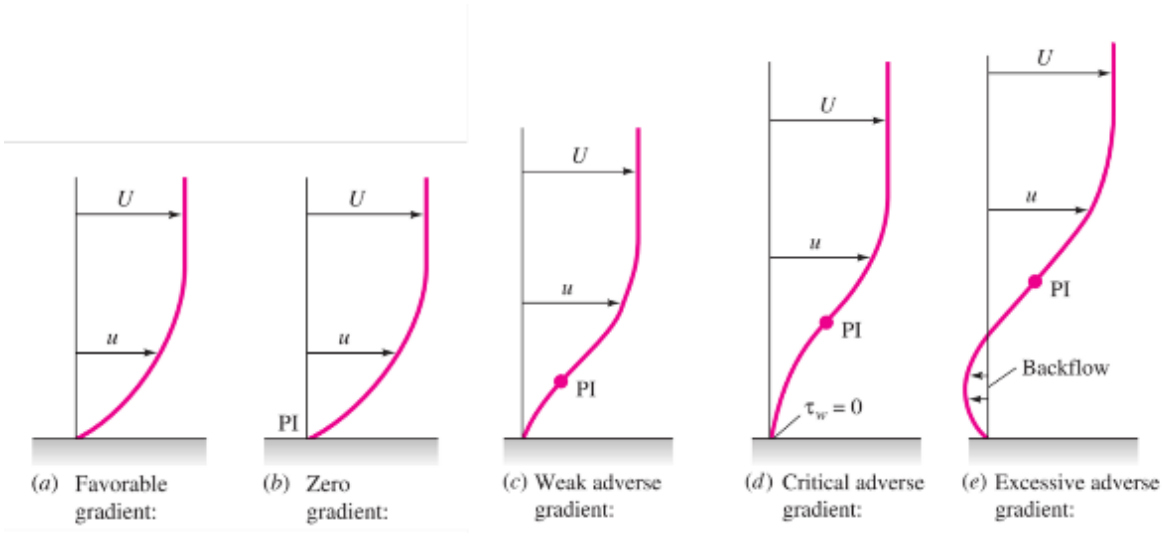

Figure 17 Boundary Layer Common Shapes According to Pressure Gradient, from [60]

In the case of compressors, the boundary phenomena will limit the amount of pressure increase that each stage can have; because at high pressure ratios backflow will occur, thereby creating stalling conditions that can compromise the machine. Turbines work with a favorable pressure gradient, so backflow will not occur; therefore, turbines are able to operate with higher pressure ratios at each stage. This is the reason why gas turbine engines have fewer turbine stages than compressor stages. High-pressure ratios in a turbine will lead to choking; at this point, the non-dimensional mass flow rate will be fixed for the entire machine. When a turbine is at its choking point, the angular speed will have no effect on the operation point; hence, it will operate as a steady machine unless the pressure ratio is drastically decreased, or the flow area is changed.

3.2.1 Choking

Choking and boundary layer separation are the most important phenomena that limit the operation of a turbomachine; they define the margins of the operation maps, and in the case of boundary layer separation, it is the main cause of losses in a turbomachine.

When the flow passes through the smallest area of a duct or passage, commonly known as throat, and this being the exact point when the flow Mach number becomes sonic, the mass flow rate passing through this object cannot be increased unless the area of this throat is changed [60]. When this occurs, the object is said to be choked and the flow has reached its maximum mass flow rate. Choking gives the shape to operation maps, as will be explained in section 3.3.

3.2.2 Incidence Angle Effect

When the compressor is working at its design point, the inlet flow angle of the next stage is almost parallel to the camber line of the blade, this creates a smooth pressure distribution on the blade and the fluid deflection, also known as turning, is achieved by the blade shape, as seen in Figure 18 A. When this happens, the compressor presents the least amount of possible losses. When the compressor works with speeds or mass flow rates that are far from the design point, the incidence angle of the fluid on the blades increases by either a positive or negative amount, as can be seen in Figure 18. The pressure distribution on the blades changes, and this can cause flow separation. At an elevated level, even flow stall. Typically, compressor blades need to have an incidence angle tolerance of +- 5° for off-design operation [55]. When the incidence angle is positive, as in Figure 18 B, the compressor stage is loading. The work done by that stage, is higher, and the deflection is increased. During positive incidence angle operation, the main flow will hit the pressure surface of the blade and the flow on the suction surface will accelerate at the leading edge. The flow will then decelerate to a speed similar to the main flow speed, creating very high local diffusion at the front of the blade. When the incidence angle is negative, the flow accelerates around the leading edge of the blade onto the pressure surface; the pressure distribution of both sides of the blade swaps. This increases the diffusion on the pressure surface. During negative incidence angles, the compressor operates under low loading. Hence, the fluid deflection is reduced, and at very high values the flow will separate causing losses and potentially stalling.

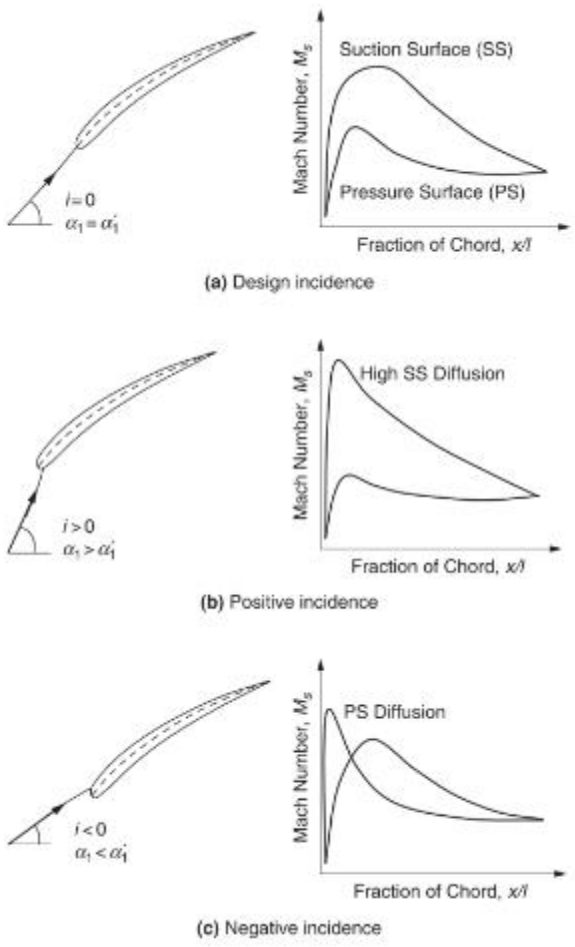

Figure 18 Incidence Angles Effects on Compressor Blades, from [55]

In a turbine, the flow is accelerating, and the pressure is falling. This produces more stable boundary layers, and thus, a turbine can accept a much higher loading without the risk of flow separation. The diffusion on a turbine is very low unless the Reynolds number is very small [55]. It is common to have supersonic speeds at the outlet of a turbine, this can cause losses due to shockwaves.

3.3 Turbomachinery Maps

All of the concepts seen so far in Chapter 3 are the main physical phenomena that occur in a turbomachine. As mentioned in Chapter 1, to compute all of them requires a huge amount of computational power and time. Turbomachinery maps contain all the information mentioned before in this chapter, the data is shown in a practical way and can be used to model the behaviour of a machine. The turbomachine maps are graphical tools that show the operational and the performance

data of a machine at different conditions of angular speed, mass flow rate, pressure ratio, and efficiency. The maps are made through expensive empirical tests and are owned by turbomachinery manufacturers. Given that the maps contain confidential information; they are typically difficult to obtain. One of the reasons that this work uses turbomachinery maps, as mentioned in Chapter 1, is that when two machines are of the same type, geometrically similar, and work with the same fluid, then the maps of one can be used to represent the other [62] [63].

There are two types of compressor maps, the ones based on pressure ratio and mass flow rate, in this work referred as operation maps; and the ones based on efficiency and mass flow rate, in this work called performance maps. The compressor operation map has mass flow rate as the x-axis and pressure ratio as the y-axis. It has several number of curves, each one represents a constant angular speed. This is illustrated in Figure 19. These curves are limited at the left of the map by the surge line and at the right by the stall line. Surge and stall conditions are explained later in section 3.3.1.

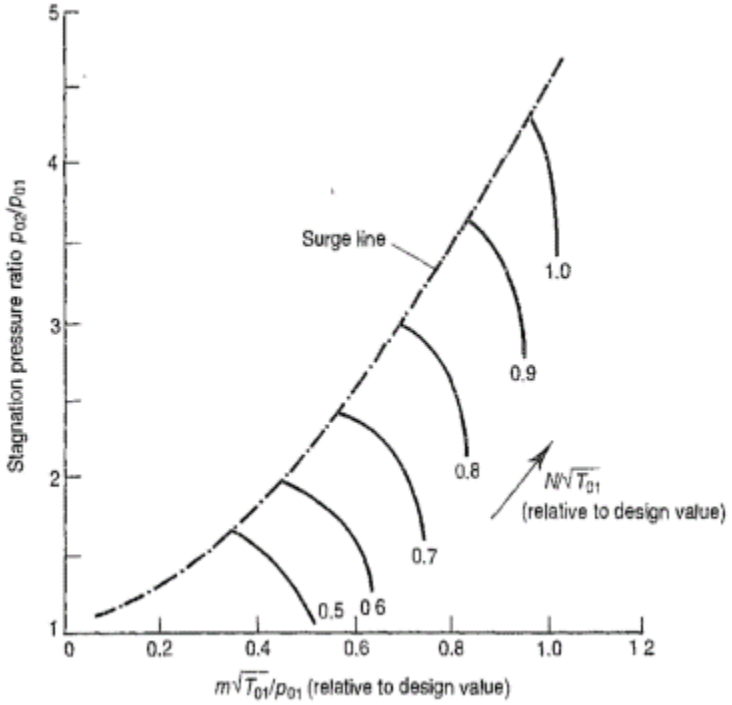

Figure 19 Typical Compressor Operation Map, from [57]

Compressor maps usually do not contain data from speed values below 50% of the nominal speed, because at these low speeds the operation of the compressor is not stable and makes it very complex to obtain data from it [49]. As can be seen in Figure 19, all the speed curves in the map tend to become vertical at high mass flow rates, this is because the first stages of the machine become

chocked and the mass flow rate cannot be increased [55]; choking conditions are explained in section 3.2.1. In an compressor efficiency map, mass flow rate is used as the x-axis, isentropic efficiency is the y-axis and again different constant speed curves are plotted.

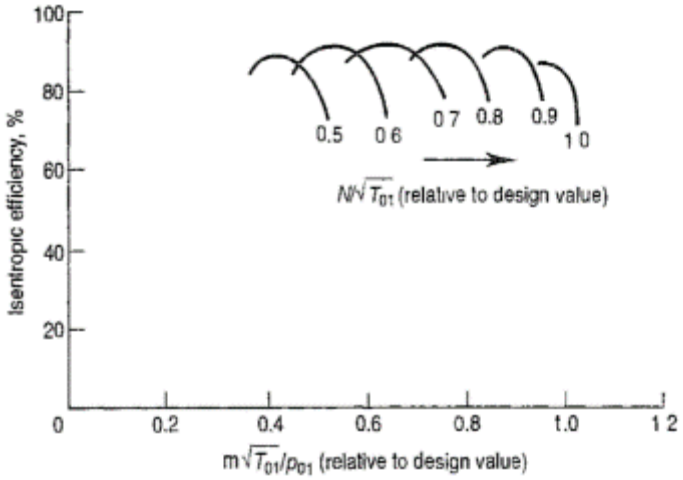

Figure 20 Typical Compressor Performance Map , from[57]

Turbine maps are also classified into two types: operation and performance. In contrast to compressor maps, turbine maps have the pressure ratio on the x-axis and not mass flow rate. The maps contain several curves of different constant speeds, similar to compressor maps.

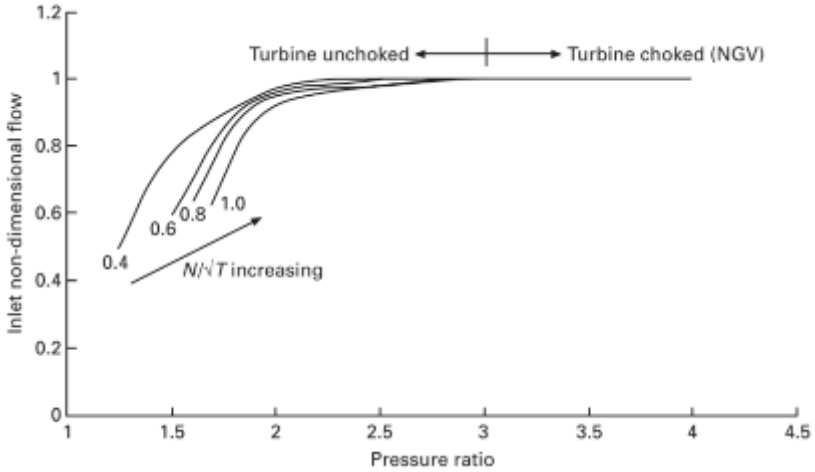

Figure 21 Typical Turbine Operation Map, from [64]

In a turbine map, all the speed lines merge into one after certain amount of pressure ratio, this is because the stator becomes choked; thus, the mass flow rate cannot be increased at this point even if the angular speed is changed.

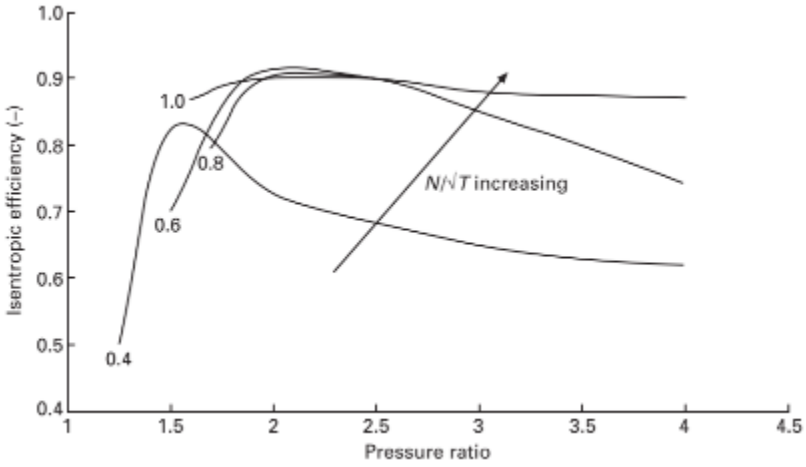

Figure 22 Typical Turbine Performance Map, from [64]

Due to the nature of both machines, compressors are usually designed to be stable at the biggest range of conditions possible, and then have the best possible efficiency; on the other hand, turbines are more stable, thus, they are designed to be the most efficient possible [56].

3.3.1 Surge and Stall

As mentioned in section 3.3, the compressor map is limited by the surge and stall lines, these lines represent two events that occur during the compressor operation. Stall occurs when the incidence angle on a compressor rotor blade reaches the point where the kinetic and potential energies cannot keep the flow without separating it, thus the back flow present due to boundary layer separation stops the rotor and creates local stall [65]. Multistage compressors can operate with some of their stages stalled; during slow speed operation, after start up, the frontal stages may be stalled and the compressor can operate normally [49]. However, the aim of a turbomachine operation is to have all its stages moving. Surge, is the point where the local stall is so severe that the machine cannot produce the pressure rise needed; which then, reverses the flow from high to low pressure. This produces a loud bang. If this happens, bleed valves must be opened to prevent this phenomenon from happening again; if no action is taken, the cycle repeats five to ten times a second [49]. Surge eventually creates engine damage. For these reasons, turbomachinery-controllers always work to prevent these phenomena, and the range of operation conditions of a machine is reduced.

This chapter has attempted to provide the reader the necessary information to understand how turbomachines work, and why the author decided to use turbomachinery maps in the models. The complexity of the phenomenon occurring inside the machines is without a doubt a significant challenge to model; the maps help notably to keep the results realistic. The next step to carry out is connecting this information with time, in order to obtain a dynamic model. Chapter 4 contains the details of how the model is built, and how the simulation is performed.

Chapter 4
Compressor and Turbine Models

This chapter details the turbomachinery models developed in this work. Due to the size of the models, and the large number of components that it contains, this chapter is divided into three different sections. The first section, section 4.1, contains the compressor and motor model; the next section, section 4.2, contains the method used to obtain the data form the compressor maps; the last section, section 4.4, contains the turbine model .

4.1 Compressor Model

A realistic and accurate simulation of an axial compressor is a very complex task because these machines involve a fluid moving in three dimensions. Since the fluid is not moving uniformly at every stage, it has different speeds and different directions, thereby making the modelling of the process very complex. As mentioned in Chapter 1, CFD modelling requires an enormous amount of computational power and time to obtain a realistic result, also it is not possible to connect a CFD model to a controlling model which is one of the goals of this work; for this reason, this model uses compressor maps; which are made by empirical tests and contain an accurate representation of what happens inside a turbomachine.

4.1.1 Compressor Model Equations

As mentioned in section 3.3, there are two types of compressor maps; operation maps, which show pressure ratio as a function of the mass flow rate with curves of constant angular speed, as seen in equation (14) ; and performance maps, which show isentropic efficiency as a function of mass flow rate and constant angular speed curves, as seen in equation (15) .

$$Pr(\dot{m}, \omega) \tag{14}$$

$$\eta_{isen}(\dot{m}, \omega) \tag{15}$$

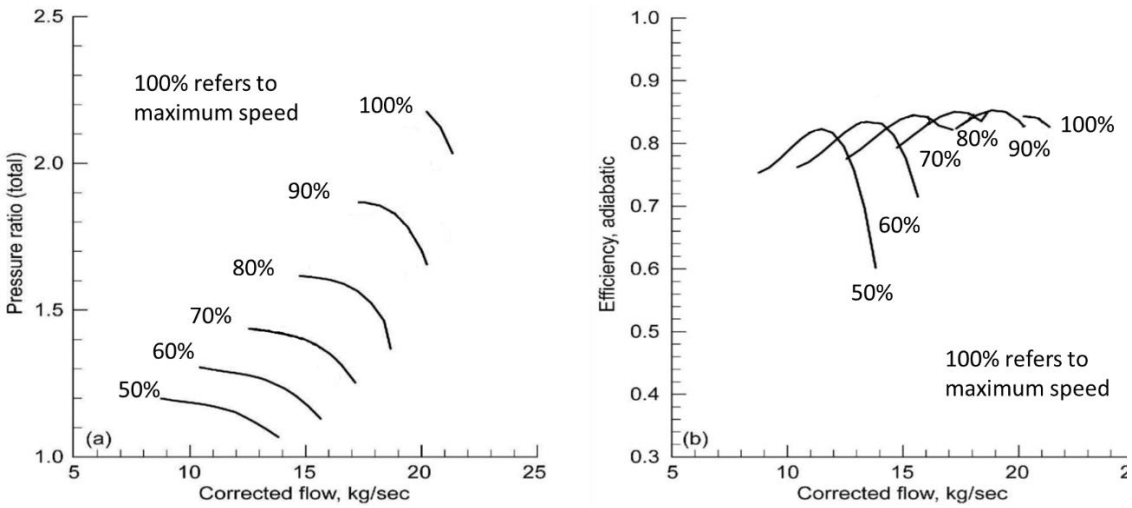

Figure 23 NASA 37 Compressor Maps, from [66]

To connect the thermodynamics of a compressor to the rotational motion of the system, the next equation is used, from [57]

$$I\frac{d\omega}{dt} = Motor\ Torque - Load\ Torque - Friction\ Torque \tag{16}$$

The equation is derived from Newton's second law; in it, I represents the moment of inertia of the machine and of the motor that is spinning it. Load torque, is the force that the fluid is exerting on the machine, which is the force normal to the one that the rotor is exerting on the fluid; friction torque is the mechanical friction produced by the bearings and other solid components of the motor and compressor. Equation (16) indicates that the difference between torques will accelerate or decelerate the motor; if no difference is present, the system will keep a constant speed. When multiplied by the angular speed, equation (16) becomes a power based equation, leading to the next equation, from [57]

$$I\frac{d\omega}{dt}\omega = Motor\ power - Load\ - Friction\ power \tag{17}$$

The load is obtained by the equation (18), from [67].

$$\dot{m}\Delta h \tag{18}$$

Which is a common equation used in thermodynamics to represent the power of a compression or expansion process. In this equation $\dot{m}$ is the mass flow rate passing through the compressor, and for this work, it is considered to be uniform along the machine; Δh is the change of enthalpy produced on the fluid by the compression process. The friction power is obtained by equation (19), from [68].

$$F\omega^2 \tag{19}$$

Where F is a friction factor commonly given by the manufacturer; for this work, the friction factor is taken from [68], because this publication contains information from the Huntorf CAES plant. The motor power is the electric power supplied to the motor multiplied by the efficiency of the motor, from [68].

$$P_{electric}\,\epsilon_{motor} \tag{20}$$

Combining equations (17),(18),(19), and (20) equation (21) is obtained, from [68].

$$\frac{d\omega}{dt} = \frac{P_{electric}\,\epsilon_{electric} - [\dot{m}\Delta h + F\omega^2]}{\omega\, I} \tag{21}$$

The moment of inertia, I, in equation (21) is representative of the motor and compressor, this value is a constant, and for this work it is obtained from [68]. To obtain Δh, the temperature at the exit of the compressor is needed, it is obtained from equation (22), from [43].

$$T_2 = T_1 + T_1\left[\left(\frac{P_2}{P_1}\right)^{\frac{k-1}{k}} - 1\right]\frac{1}{\eta_{isen}} \tag{22}$$

Where T_1 is the ambient temperature, P_1 the ambient pressure, P_2 the compressor outlet pressure, and η_{isen} the isentropic efficiency. η_{isen}, is obtained from the compressor performance map. P_2, which is given by the system, is the pressure of the cavern; the ideal gas equation of state obtains it, as seen in equation (23) . The cavern is assumed to be an isothermal pressure vessel, this is because the scope of this work does not include the cavern's model. The cavern pressure is obtained from the ideal gas equation of state, as in equation (23) .

$$P_{2compressor} = P_{cavern} = \frac{m_{cavern}RT_{cavern}}{V_{cavern}} \tag{23}$$

Where R is the gas constant, T_{cavern} is the cavern temperature, V_{cavern} is the cavern volume and m_{cavern} is the mass in the cavern. The mass in the cavern is calculated with the next equation

$$m_{cavern} = \int \dot{m}_{in} - \dot{m}_{out} \tag{24}$$

In equation (24), $\dot{m}_{in}$ is the mass flow rate through the compressor going into the cavern, and $\dot{m}_{out}$ is the mass flow rate leaving the cavern. A representation of this model is shown on Figure 24.

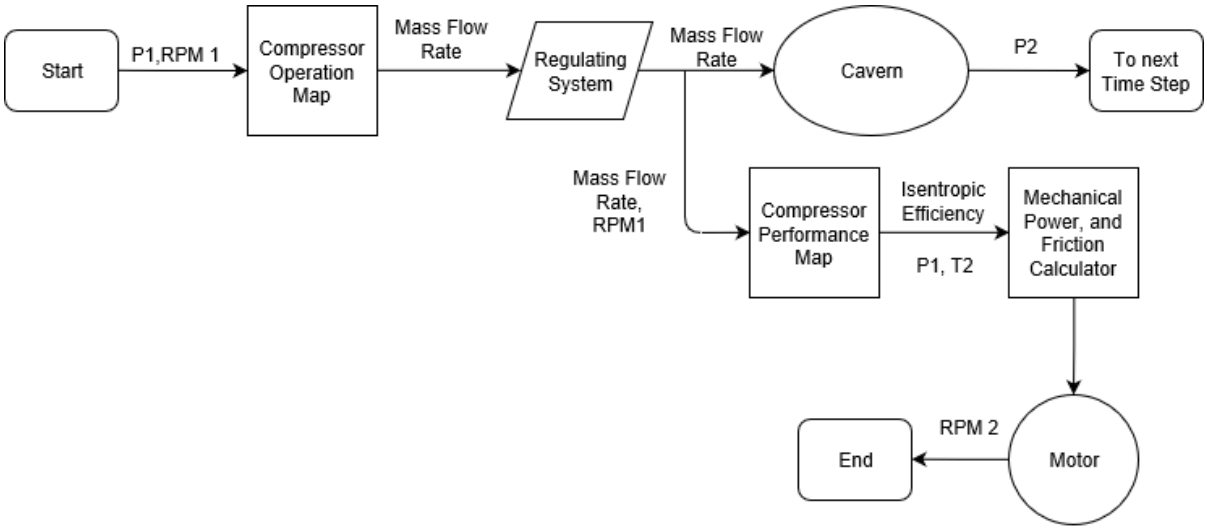

Figure 24 Compressor Model Diagram

4.1.2 Motor Equations

The compressor is driven by a three-phase asynchronous motor. In this model, during start-up, no mass can enter the compressor until it reaches the speed required to obtain the exit pressure that matches the actual cavern pressure. During this time, the compressor's rotor will spin only accordingly to the motor characteristics. After that, the valves open, letting the mass to flow across the machine. To model the motor, the asynchronous machine block from SIMULINK® is used; the following parameters need to be provided: rated power, voltage, frequency, stator's resistance and inductance, rotor's resistance and inductance, mutual inductance, inertia constant, friction factor, and number of poles. The mechanical section of the motor is calculated with equation (16), load and friction torque come from equations (18) and (19) dividing them by the angular speed. To obtain the electrical torque, the following system of equations is used[1], from [69].

$$V_{qs} = R_s i_{qs} + \frac{d\phi_{qs}}{dt} + \omega\phi_{ds} \tag{25}$$

where V_{qs} is the stator voltage of the q axis and is obtained from the sum of the product of the stator resistance R_s and the q axis stator current i_{qs}; plus, the back electromotive force on the q axis $\frac{d\phi_{qs}}{dt}$; plus, the product of the angular speed, ω, and the d axis stator flux ϕ_{ds}.

$$V_{ds} = R_s i_{ds} + \frac{d\phi_{ds}}{dt} + \omega\phi_{qs} \tag{26}$$

[1] These equations where obtained from MATLAB ® literature, the author decided to keep the same symbols for consistency.

Where V_{ds} is the stator voltage of the d axis, and is analogous to V_{qs} from equation (25); the rest of the elements of this equation are also analogous to the ones mentioned in equation (25).

$$V'_{qr} = R'_r i'_{qr} + \frac{d\phi'_{qr}}{dt} + (\omega - \omega_r)\phi'_{dr} \tag{27}$$

Where V'_{qr} is the voltage at the q axis of the rotor, and is obtained from the sum of the product of the rotor's resistance R'_r and the rotor's q axis current i'_{qr}; plus, the electromotive force of the rotor's q axis $\frac{d\phi'_{qr}}{dt}$; plus, the product of the difference between the electrical angular velocity and the reference angular velocity $(\omega - \omega_r)$, times the flux on the rotor's d axis ϕ'_{dr}.

$$V'_{dr} = R'_r i'_{dr} + \frac{d\phi'_{dr}}{dt} + (\omega - \omega_r)\phi'_{qr} \tag{28}$$

Like equation (27), equation (28) shows V'_{dr} which is the voltage at the rotor's d axis, the elements that form equation (28) are the same as in equation (27), with the axis inverted.

$$T_e = 1.5p\left(\phi_{ds} i_{qs} - \phi_{qs} i_{ds}\right) \tag{29}$$

Where T_e is the electromagnetic torque and is obtained from the difference between the stator flux of the d axis, times the current on the stator's q axis, $\phi_{ds} i_{qs}$, and the flux of the stator's q axis times the current on the stator's d axis, $\phi_{qs} i_{ds}$; this, multiplied by 1.5 times the number of poles.

$$\phi_{qs} = L_s i_{qs} + L_m i'_{qr} \tag{30}$$

Where ϕ_{qs} is the stator's electromagnetic flux on the q axis, and is obtained by the sum of the product of the total stator inductance, L_s, times the stator's q axis current; plus, the product of the magnetizing inductance, L_m, times the rotor's q axis current.

$$\phi_{ds} = L_s i_{ds} + L_m i'_{dr} \tag{31}$$

Where ϕ_{ds} is the stator's d axis electromagnetic flux, which is obtained by the sum of two products, the first product being the total stator's inductance times the stator's d axis current; the second one being the magnetizing inductance times the rotor's d axis current.

$$\phi'_{qr} = L'_r i'_{qr} + L_m i_{qs} \tag{32}$$

Equation (32), shows that the rotor's q axis flux, ϕ'_{qr}, is obtained by the sum of the product of the rotor's total inductance, L'_r, times the rotor's d axis current; and the product of the magnetizing inductance times the current at the stator's q axis.

$$\phi'_{dr} = L'_r i'_{dr} + L_m i_{ds} \tag{33}$$

Similar to equation (32), equation (33) obtains the rotor's d axis flux; which is obtained by the sum of the product of the rotor's total inductance times the rotor's d axis current, plus, the product of the magnetizing inductance times the stator's d axis current.

$$L_s = L_{ls} + L_m \tag{34}$$

Equation (34) calculates the stator's total inductance L_s, which is obtained by the sum of the stator's leakage inductance, L_{ls}, and the magnetizing inductance.

$$L'_r = L'_{lr} + L_m \tag{35}$$

Equation (35) calculates the rotor's total inductance, L'_r, by the sum of the rotor's leakage inductance, L'_{lr}, and the magnetizing inductance. The motor' equivalent diagram is shown on Figure 25.

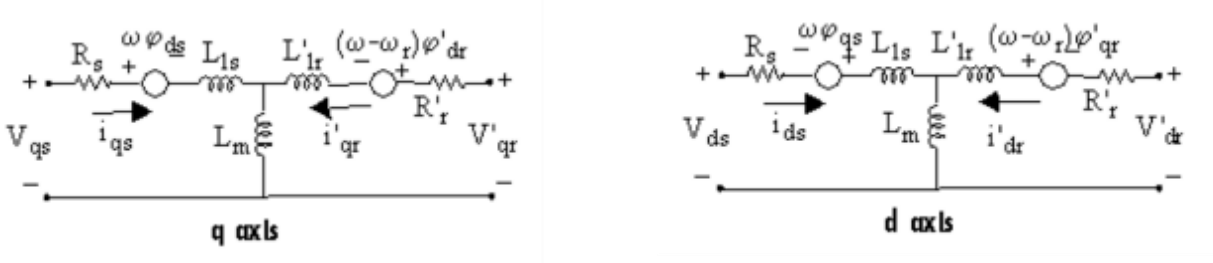

Figure 25 Induction Motor Equivalent Diagram, from [69]

4.1.3 Compressor Model Solving Sequence

The model is solved numerically using MATLAB® and SIMULINK®; the initial conditions required from the user to solve the model are P_1, T_1, P_{cavern}, cavern volume, the motor speed at which the valve opens, and the initial angular speed which is any number greater than zero. For this work the initial speed selected is 1% of the compressor's nominal speed.

After the initial conditions are given and the motor specifications provided, equation (16) is solved at each time step considering the load torque as zero until the speed at which the valve is opened is reached. Once the opening valves speed has been reached, the mass flow rate is calculated through the compressor map using the current angular speed of the rotor and the pressure ratio between the cavern and the ambient pressure. After the mass flow rate is known, it is then used as input to the efficiency compressor map to calculate the isentropic efficiency. After that, the temperature at the end of the compressor is calculated by equation (22), and the new cavern pressure by equation (23). After that, the temperature at the compressor's outlet is used to calculate the work done by the compressor

and is supplied to equation (16) to calculate the angular speed of the next timestep. A visual representation of this process is shown in Figure 26.

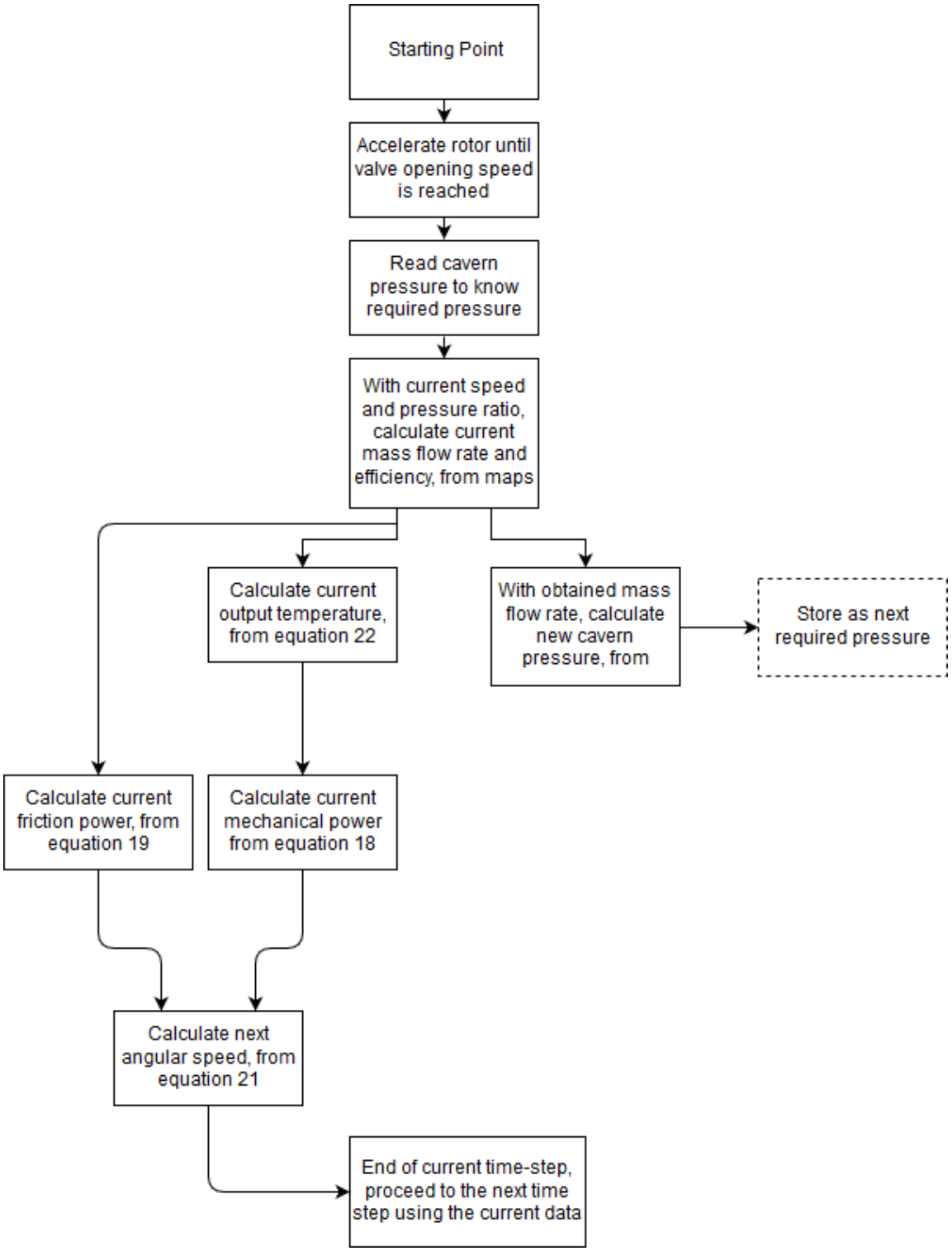

Figure 26 Compressor Simulation Solving Sequence

4.2 Beta Lines

As seen in Chapter 1, one known drawback of using compressor maps is the difficulty of reading data from the map due to its complex shape. For this reason, in this work, beta lines like the ones in [48], shown in section 2.2, are created. To obtain the beta lines, the higher point of each speed line and the origin of the graph are taken as data to fit a parabolic curve, as seen on Figure 27, this way the first beta line is obtained.

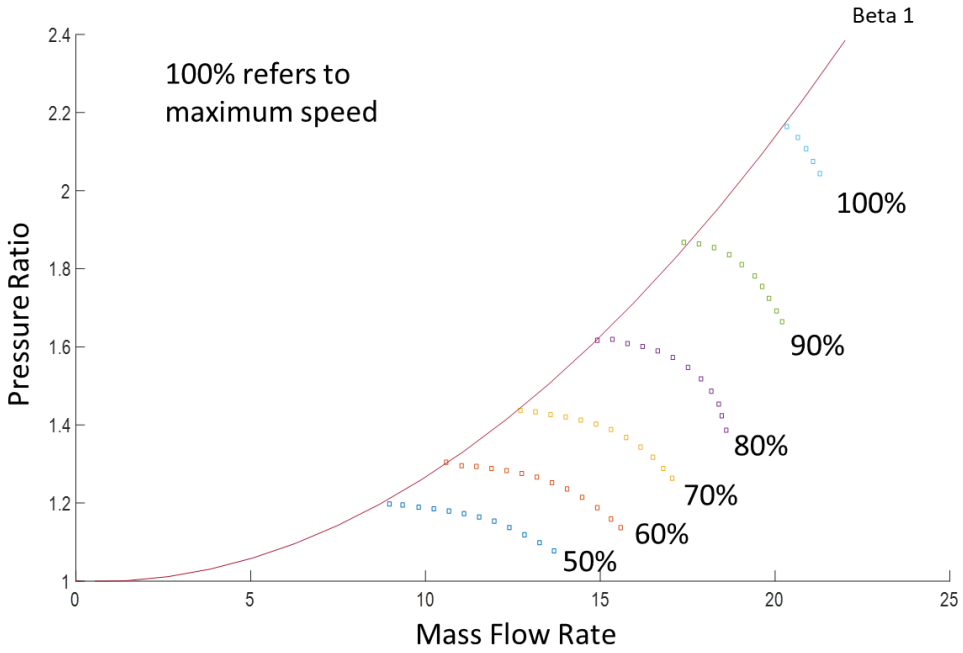

Figure 27 Compressor NASA-37 Operation Map with First Beta Line

The first beta line complies with the equation form $A\ x^2 + B\ x + C$; to obtain the other beta lines, the value of B is increased in equally spaced intervals to cover the area between the first beta line and the stall limit of the compressor map. The achieved result is shown on Figure 28.

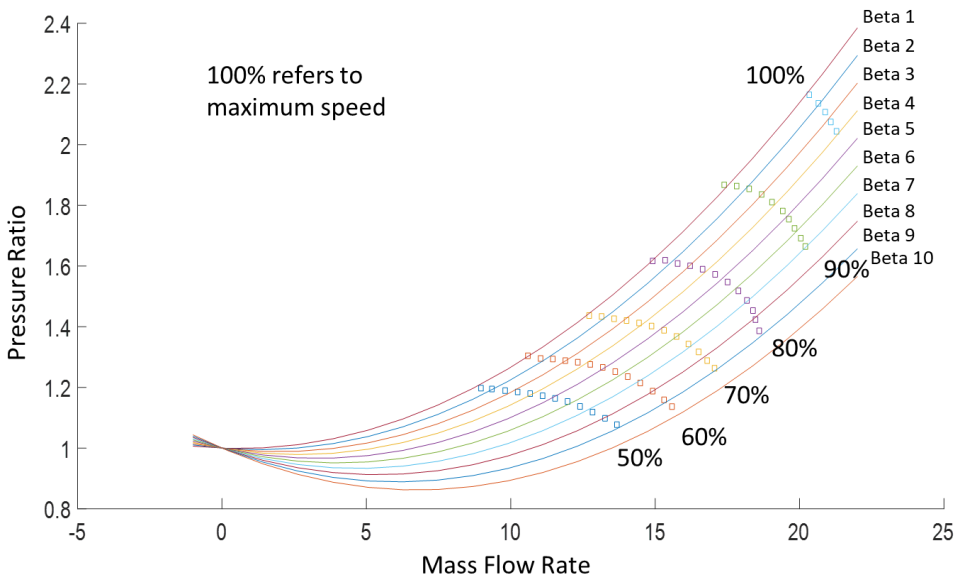

Figure 28 Compressor NASA-37 Operation Map with full Range of Beta Lines

After the map is fully covered, multiple data points are read per beta line to build two tables. The tables have the beta line number as the header of each column, the angular velocity values as the header of each row; and in the interior, either the pressure ratio or the mass flow rate; as seen on Table 1 and Table 2.

Table 1 Pressure Ratio Beta Lines Data for Compressor NASA-37

		Beta Line Number									
		1	2	3	4	5	6	7	8	9	10
Speed %	50	1.1965	1.1926	1.1857	1.1759	1.1641	1.1454	1.0993	1.0669	1.0679	1.0267
	60	1.3004	1.2886	1.2866	1.2777	1.263	1.2424	1.1865	1.1512	1.1502	1.108
	70	1.4395	1.4267	1.4198	1.409	1.3914	1.3659	1.2972	1.256	1.254	1.204
	80	1.6178	1.6129	1.5992	1.5835	1.5589	1.5246	1.4265	1.3657	1.3648	1.2893
	90	1.8599	1.8628	1.8344	1.802	1.7657	1.7127	1.5902	1.5127	1.5019	1.4255
	100	2.1706	2.1333	2.0853	2.0372	1.9607	1.8862	1.7186	1.6225	1.595	1.5186

Table 2 Mass Flow Rate Beta Lines Data for Compressor NASA-37

		Beta Line Number									
		1	2	3	4	5	6	7	8	9	10
Speed %	50	8.662	8.662	10.037	10.695	11.372	12.079	13.231	13.782	13.812	14.131
	60	10.579	10.579	11.885	12.563	13.221	13.831	14.915	15.389	15.379	15.815
	70	12.669	12.669	13.918	14.576	15.157	15.738	16.676	17.112	17.112	17.412
	80	14.886	14.886	16.183	16.783	17.315	17.780	18.448	18.631	18.622	18.651
	90	17.451	17.451	18.690	19.135	19.541	19.899	20.354	20.412	20.287	20.393
	100	20.258	20.258	20.983	21.361	21.467	21.574	21.709	21.632	21.332	21.467

These tables are then created using a block called “Look-up Table (n-D)”, where they are used as look- up tables, and linear interpolation is used to find values to feed into the model.

4.3 Map Scaling

Turbomachinery maps are a valuable asset of turbomachinery manufacturers. Very expensive experiments need to be conducted in order to create these maps. Therefore, it is very hard to acquire a specific one. The probability of finding a map that exactly fits the required conditions for the system to be modeled, i.e., pressure ratios, mass flow rates, efficiencies, is very low. However, scaling maps of an existing machine is a practice that has been done for many years with good results [49], [62], [70]–[72]. The scaling methods available in the literature vary from simple linear methods to complex iterative algorithms [71], [73]–[79]. After reviewing the above mentioned methods, and analyzing the complexity and clarity of the publications; the method proposed by Kong et al, which according to the authors has an accuracy error of 6% or less [74], is chosen for this project. The method is divided in two parts; the first part consists on obtaining linear scaling factors; to obtain these, equations (36) (37) and (38) are used.

$$PR_{factor} = \frac{PR_D - 1}{PR_{MD} - 1}(PR_M - 1) + 1 \tag{36}$$

Where PR_{factor} is the pressure ratio factor relation between the original and the scaled map. PR_D is the desired pressure ratio of the scaled map, PR_{MD} is the pressure ratio at the design point of the original map, and PR_M is an arbitrary pressure ratio of the original map.

$$\dot{m}_{factor} = \frac{\dot{m}_D}{\dot{m}_{MD}}\dot{m}_M \tag{37}$$

Where $\dot{m}_{factor}$ is the mass flow rate factor relation between the original and the scaled map, $\dot{m}_D$ is the desired mass flow rate of the scale map, $\dot{m}_{MD}$ is the mass flow rate at the design point of the original map, and $\dot{m}_M$ is an arbitrary mass flow rate of the original map.

$$\eta_{factor} = \frac{\eta_D}{\eta_{MD}}\eta_M \tag{38}$$

Where η_{factor} is the efficiency factor relation between the original and the scaled map, η_D is the desired efficiency of the scale map, η_{MD} is the efficiency at the design point of the original map, and η_M is an arbitrary efficiency point of the original map. The values chosen to obtain the factors are shown in Table 3. In the second part of the method, each component of the beta lines obtained in section 4.2; pressure ratio, mass flow rate, efficiency, is plotted against their respective rotational speed. Then, each of the curves of these plots is fitted into polynomial equations. The pressure ratio curves fit well to polynomial equations of second degree; efficiency and mass flow rate, fit well to polynomial equations of third degree. Figure 29, Figure 31, and Figure 30, show the fit results of the curves.

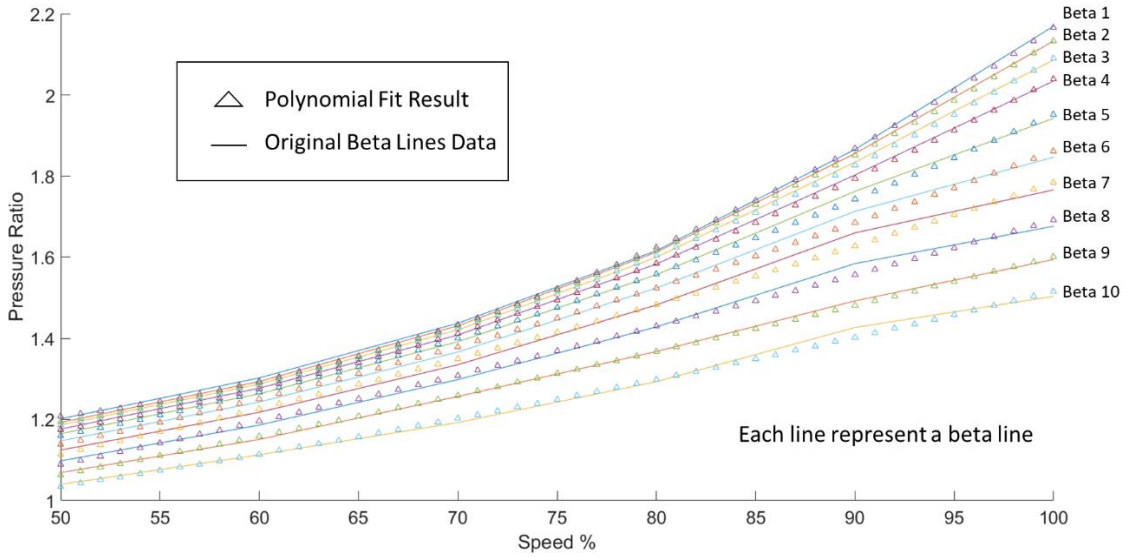

Figure 29 Compressor's Beta Lines Pressure Ratio Data Plotted Against Speed Data with Polynomial Fit Results

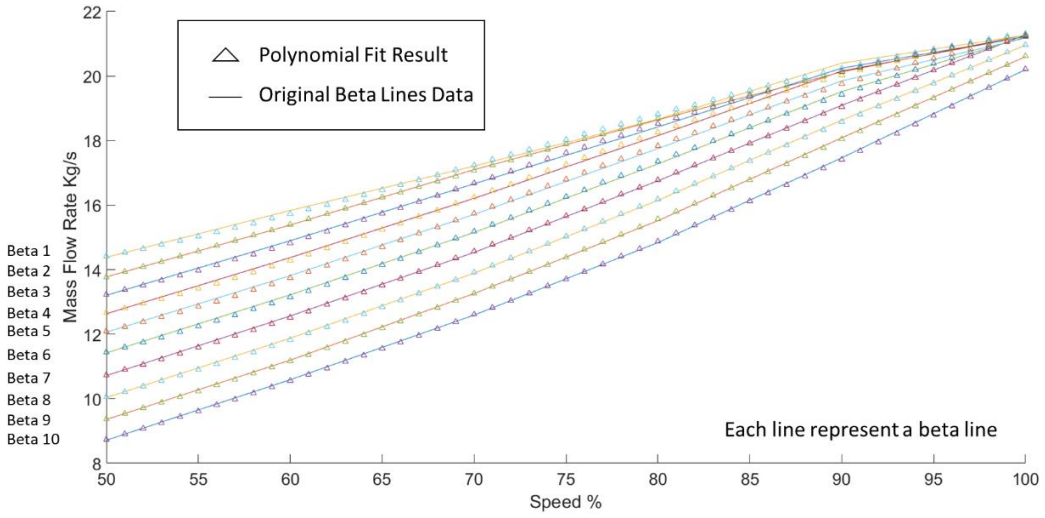

Figure 30 Compressor's Beta Lines Mass Flow Data Plotted Against Speed Data with Polynomial Fit Results

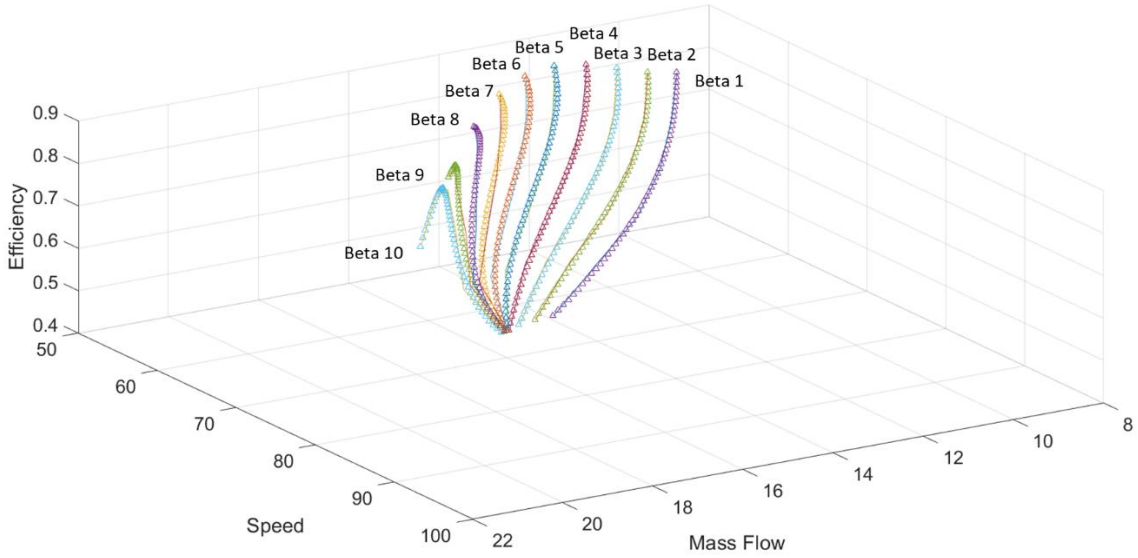

Figure 31 Compressor's Beta Lines Efficiency Data Plotted Against Speed Data with Polynomial Fit Results[2]

[2] This plot is chosen to be displayed in 3D because to ensure it is interpreted only in one way.

After the curve fitting equations for each of the beta lines are obtained, each equation is multiplied by their corresponding factor. Then this is plotted in the generic maps format, and new operation and performance maps are obtained, as seen in Figure 32 and Figure 33.

Table 3 Data used for Map Scaling

Scaling Data	Value
PR_D	6
PR_M	2.12
PR_{MD}	1.5632
$\dot{m}_D$	41.6468 Kg/s
$\dot{m}_M$	20.8234 Kg/s
$\dot{m}_{MD}$	17.2907 Kg/s
η_D	85 %
η_M	84.12 %
η_{MD}	85.19 %

The data is obtained from the original compressor map, by choosing a nominal operation point and an arbitrary point; and choosing the nominal operation point in the desired map.

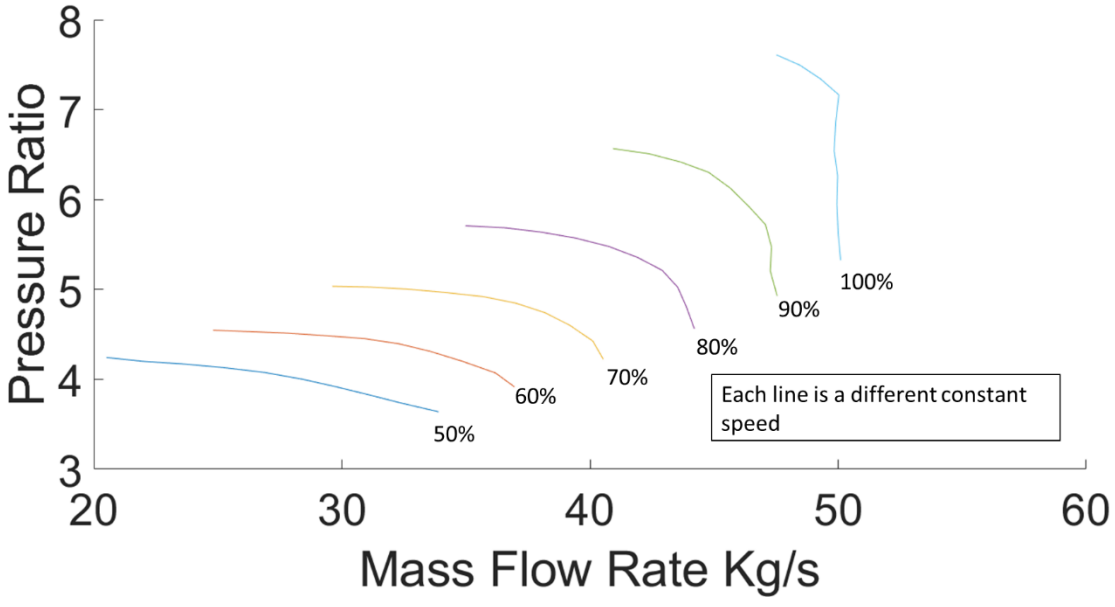

Figure 32 Scaled Compressor Operation Map

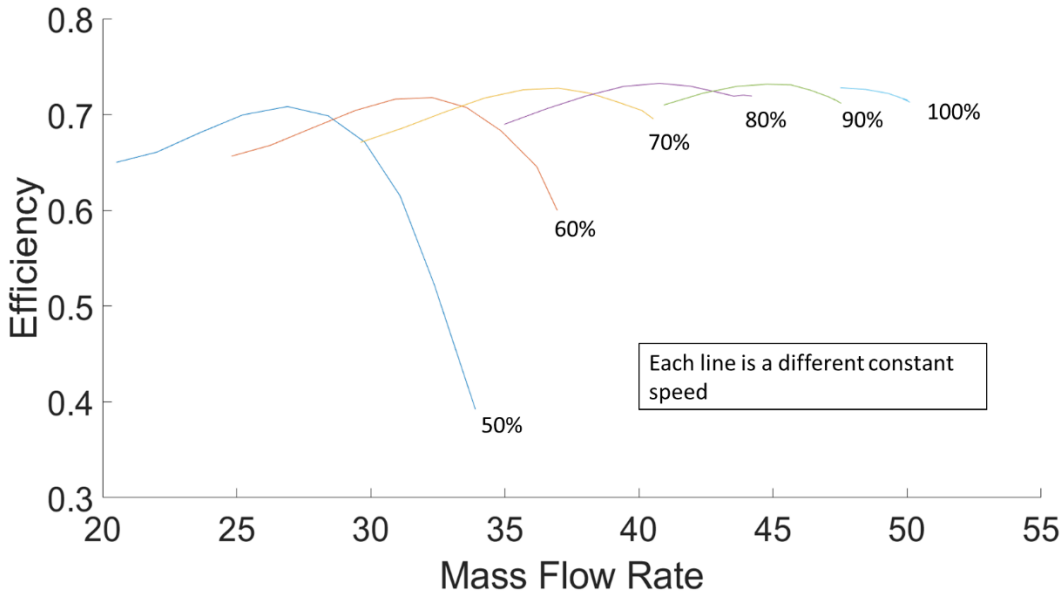

Figure 33 Scaled Compressor Performance Map

4.3.1 Compressor Regulating System

To make the simulation results more representative, a simple regulating system is added to the model to prevent it from going into surge or stall. To achieve this, the map is divided into different sections, by two parabolic lines. These lines are then interpreted as equations and the values of estimated operation points are introduced into the equations and compared to the limits. If the estimated operating point is above the upper limit, the mass flow rate is increased until the operating point is within the specified limits. If the estimated point is below the stall line, the mass flow rate is

reduced. The speed is adjusted after the mass flow rate has been regulated. The limits and lines used for this model are shown below in Figure 34.

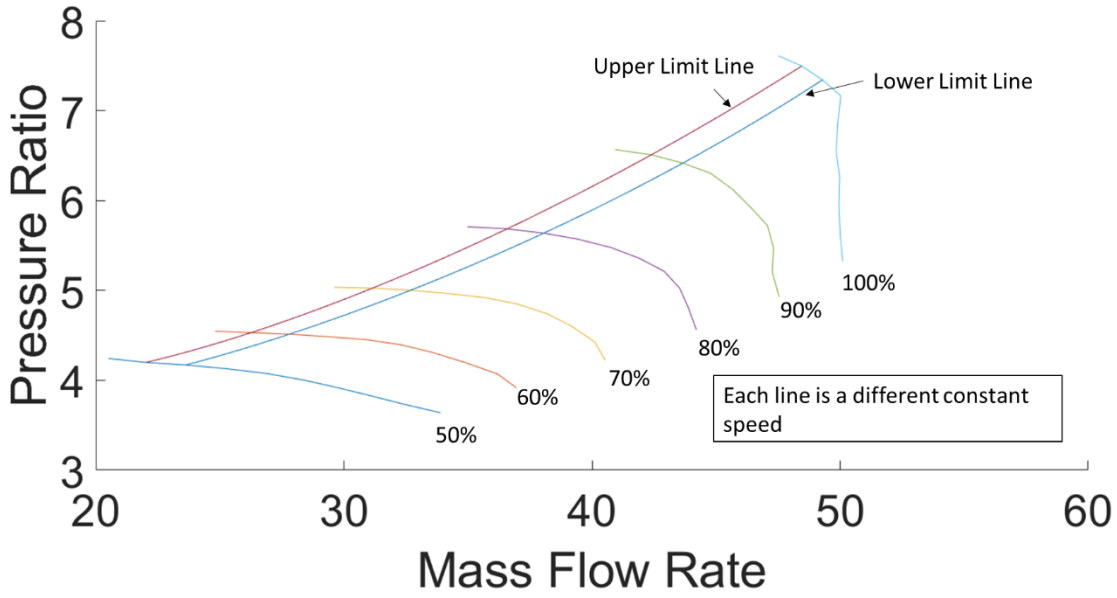

Figure 34 Compressor Regulating System Guiding Lines

4.4 Turbine Model

The turbine is modelled as a semi-steady process, i.e., the pressure at the inlet and outlet of the turbine is kept constant, and the outlet temperature varies according to the efficiency of the machine. This approach is chosen to simulate a pressure regulator installed upstream of the turbine as in the CAES plant in Huntorf, Germany [80].

4.4.1 Turbine Equations

Like the compressor, the turbine model requires turbine maps to represent the complex phenomena occurring with the flow inside it.

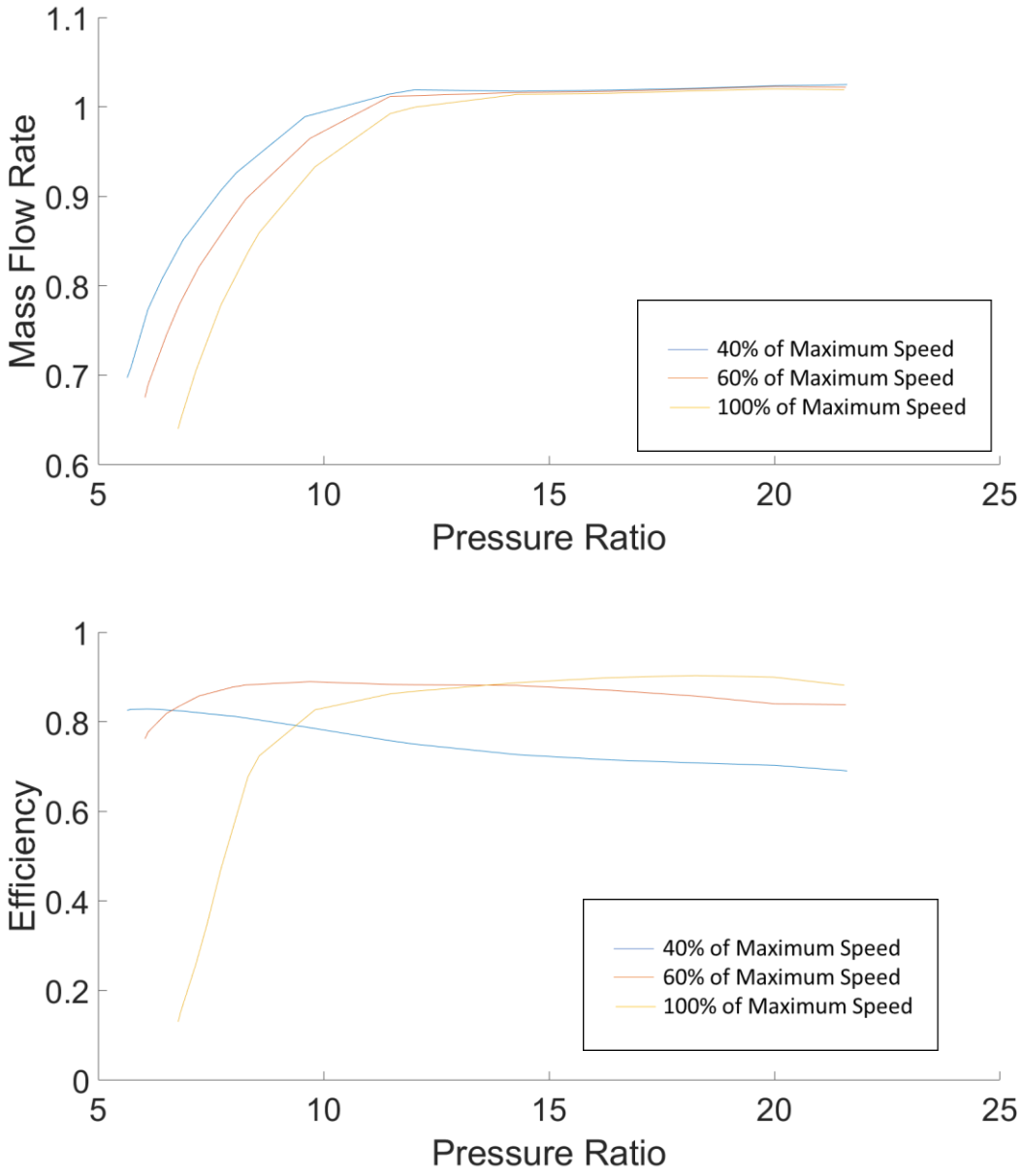

Figure 35 Turbine Maps, scaled from [57]

In Figure 35, one map shows the mass flow rate as a function of the pressure ratio and the angular velocity, same as in equation (14) used for the compressor model. The other map, describes the isentropic efficiency as a function of pressure ratio and angular velocity, as seen in equation (39) .

$$\eta_{isen} = (Pr, \omega) \tag{39}$$

To connect the thermodynamics and flow characteristics to the rotational motion of the rotor, equation (40), from [68] , is used.

$$\frac{d\omega}{dt} = \frac{Turbine\ power - \ Load\ - Friction\ power}{\omega\ I} \tag{40}$$

In this equation, turbine power refers to the power produced by the turbine, the load is a simulated electrical load connected to the rotor of the turbine, and the friction power refers to the one produced on the bearings and other solid components of the system, by applying equation (18) and equation (19) into equation (40) the next equation is obtained.

$$\frac{d\omega}{dt} = \frac{\dot{m}\Delta h - \ Load - F\omega^2}{\omega\ I} \tag{41}$$

The friction factor needs to be known beforehand, for this work this value is obtained from [68] because it is representative of the Huntorf CAES plant. The load, is the combination of a signal produced by the signal builder block, and the chosen nominal load to be supplied by the machine, i.e., after deciding the nominal load, it is multiplied by a non-constant signal that comes from the signal builder, this is done to see how the turbine reacts to a theoretical change of load.

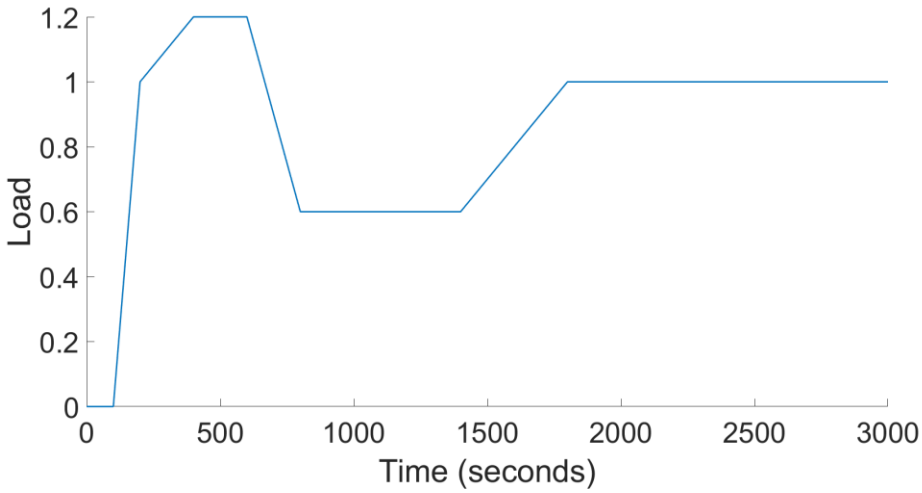

Figure 36 Arbitrary Turbine Load

The moment of inertia *I* is a constant, for this work it was obtained from [68], because it is a representation of the Huntorf CAES plant. To obtain the turbine power, the fluid's temperature at the exit of the turbine, T_4, is required, this is obtained by equation (42), from [81].

$$T_4 = T_3 - T_3\eta_{isen}\left[1 - \left(\frac{P_3}{P_4}\right)^{\frac{k-1}{k}}\right] \tag{42}$$

Where T_3 is the inlet temperature, P_3 the inlet pressure, and P_4 the ambient pressure. The isentropic efficiency and the mass flow rate are obtained from the turbine performance maps.

4.4.2 Turbine Model Solving Sequence

Like the compressor model, the turbine is solved numerically using MATLAB® and SIMULINK®. The solution starts by choosing the nominal load of the machine, nominal angular velocity, turbine's inlet pressure and the inlet temperature. An initial speed, of some value close to zero, is required to avoid mathematical errors. For the first time-step, an initial value for speed and pressure ratio is used to obtain the mass flow rate and the isentropic efficiency from the performance maps. Then, the output temperature is obtained using equation (42). The squared current speed gets multiplied to the friction factor, then the 3 quantities; load, friction and turbine power are used in equation (41) and the next angular speed is obtained to be used in the next time step. The pressure ratio is kept constant, and the process continues. A graphical representation of this process is shown in Figure 37.

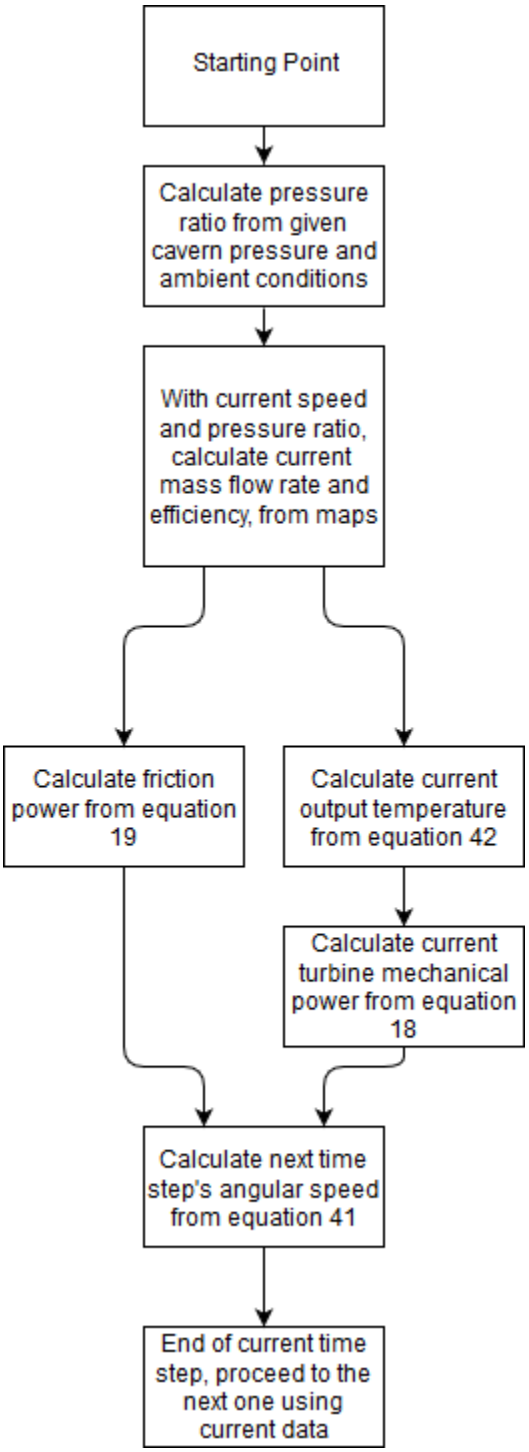

Figure 37 Turbine Simulation Sequence

The models shown in this chapter give the current conditions of both machines at each time step. The compressor time line can be delimited by the pressure ratio increment that will occur in the cavern.

The turbine time line, will depend on the cavern's pressure. This pressure is affected by the heat transfer between the cavern and its surroundings. For this reason, this topic is out of the scope of this work. However, an adiabatic or isothermal cavern can be modeled using the ideal gas equation of state, to obtain an approximation of the available time that the turbine could be producing power. The developed models in this work are unique because compression and expansion components are completely independent of each other. Furthermore, they simulate the compressor driver and the turbine load, whose effects are commonly just assumed without considering the transients. All the equations required to model the turbomachinery behaviour have been shown in this chapter. In the next chapter, Chapter 5, the results of the simulations are shown and explained.

Chapter 5
Simulation Results

The results shown in this chapter are to establish that the models behave as expected with regards to start-up behaviour, inertial effects, and fluid mechanics limits. Given there is very limited experimental data to validate against, this chapter depends more heavily on ensuring that the results match the map, and that the transient results are reasonable. This chapter is divided into two different sections: section 5.1 contains the compressor simulation results, and section 5.2 the turbine simulation results.

5.1 Compressor Simulation

5.1.1 Initial Data and Compressor maps

The compressor model in this work simulates a variable speed axial compressor. It is assumed that this compressor is connected directly to a cavern. The data and compressor maps chosen for the model are shown on Table 4, Figure 38 and Figure 39. Some of the values, as specified by the * next to them, are obtained form [68], the data from this source corresponds to values of the Huntorf CAES plant. However, this model does not fully replicate Huntorf's compressor train, which consists of an axial and a centrifugal compressor. The aim of this model is to simulate an axial compressor similar to Huntorf's. Since not enough published data is available, specifically about pressure ratios, compressor maps, and efficiencies; this work assumes that the axial compressor used in the Huntorf plant has a nominal pressure ratio of 7:1.

Table 4 Compressor Simulation Parameters

Parameter	Value
Cavern Operation	Isothermal
Cavern Volume	3000 m^3 **
Ambient Temperature	298°K
Motor Nominal Power	15.5 MW
Motor Inertia	1200 kg m^2
Motor Nominal Voltage	460 V
Motor Nominal Frequency	60 Hz
Compressor Nominal Mass Flow Rate	55 kg/s
Compressor Inertia	2400 kg m^2
Compressor's Friction Factor	3.94 *
Compressor's Nominal Pressure Ratio	7.32
Initial Cavern Pressure	422.18 Kpa
Final Cavern Pressure	747.4 Kpa

* Data obtained from [68]

** The cavern is 100 times smaller than Huntorf, to reduce simulation time

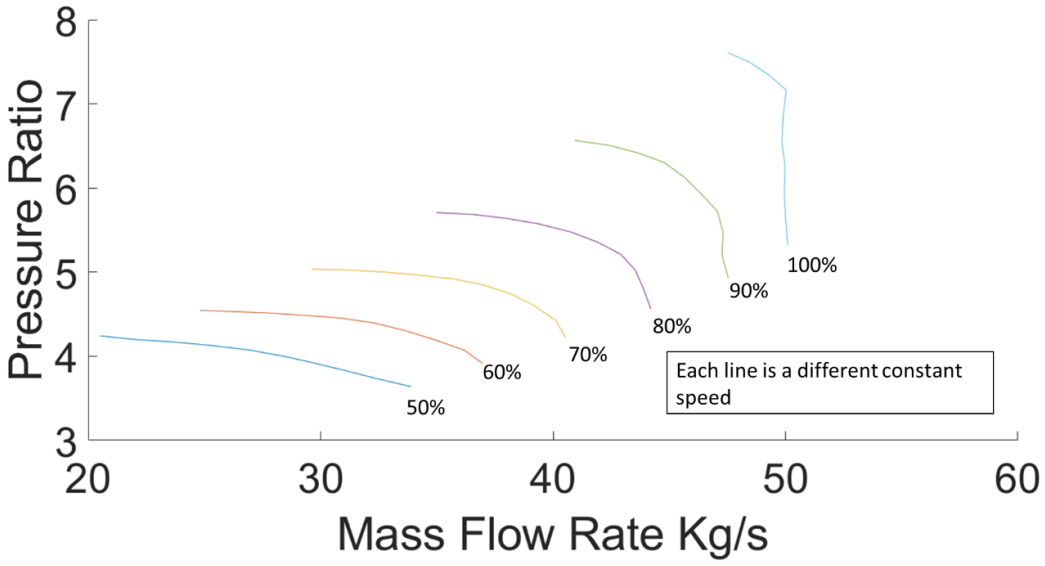

Figure 38 Scaled Compressor Operation Map

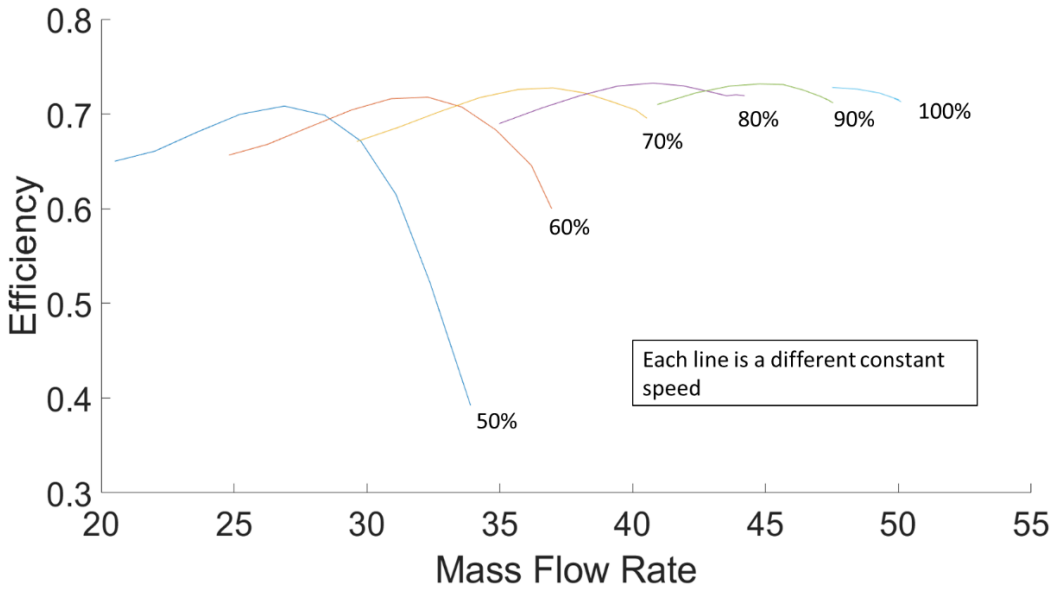

Figure 39 Scaled Compressor Performance Map

5.1.2 Simulation Time Step

The compressor model's motor section uses a block called asynchronous machine, this block represents a high fidelity physical model of the induction motor. Therefore, the block is very sensitive to changes in time steps and selection of solving method. If a time step bigger than .001 seconds is used, the shape of the sinusoidal waves used for the electrical system is distorted. Thus, preventing the simulation from running.

5.1.3 Compressor's speed

The speed at which the compressor operates is dependent entirely on the compressor's design conditions. When the mass flow valve is open, the compressor must operate within the set limits between the surge and stall lines, as can be seen in Figure 40 below.

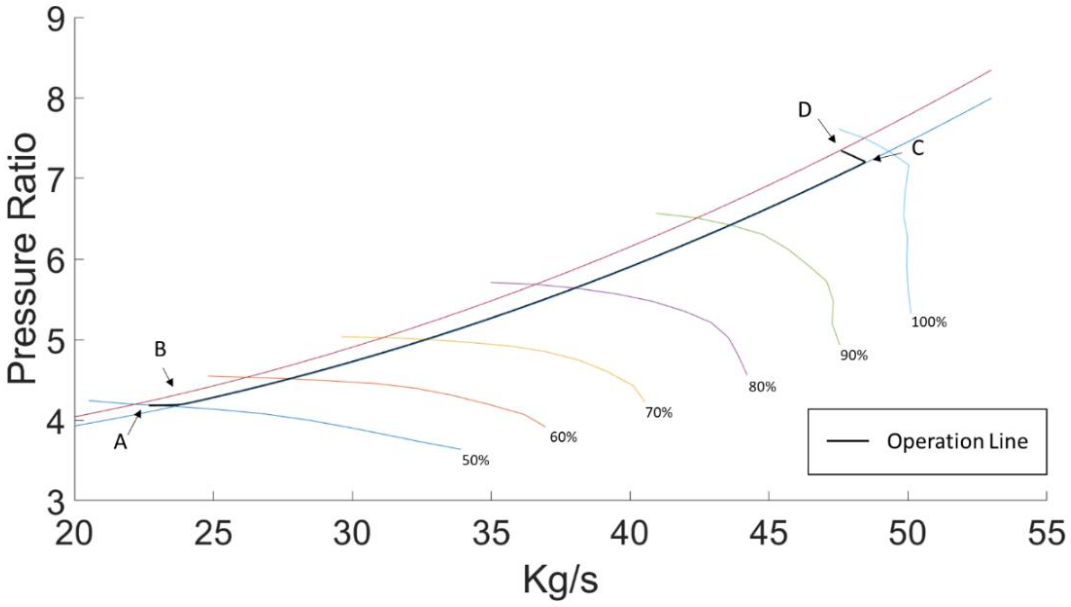

Figure 40 Operation Line Result on Scaled Compressor Map

In Figure 40, the red and blue curves are the predefined operating limits, as seen in section 4.3.1. Point A shows the mass flow valve opening, after reaching 50% of the nominal speed; the mass flow rate at this point is 22.68 kg/s. At point B, the operating point reaches the lower limit and the regulating systems stars controlling the operation. The system regulator keeps the mass flow rate within the surge and stall limits, as seen on Figure 40 from point B to point C. This is done by adjusting the speed increase according to the increment of pressure in the cavern. At point C, the system reaches its maximum speed; from there to point D, it will maintain a constant speed and the increasing backpressure from the cavern produces reduction in the mass flow rate.

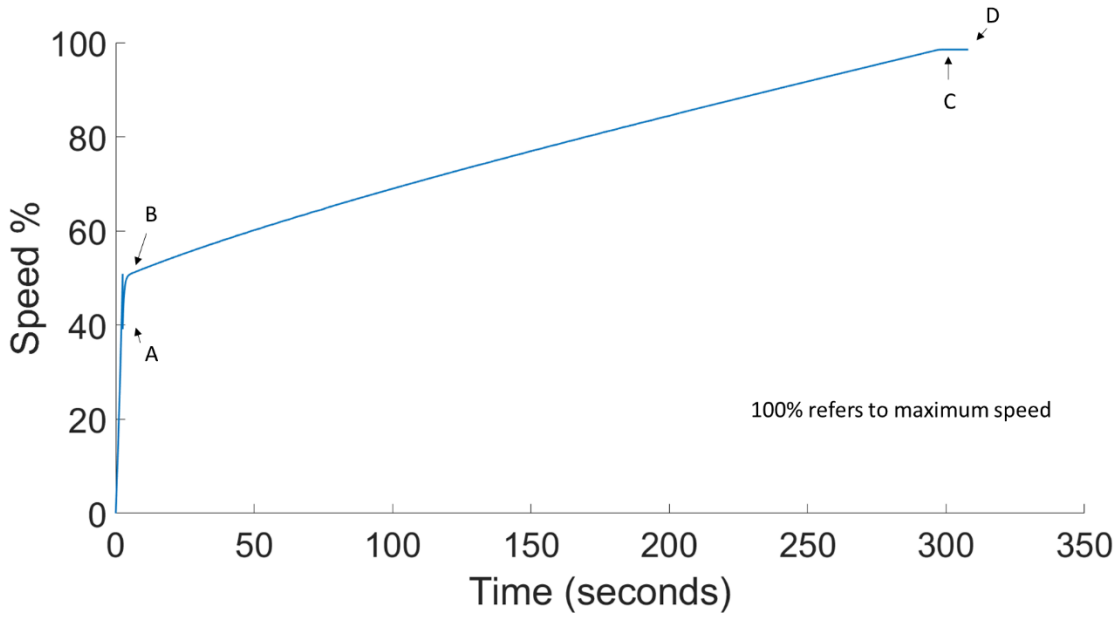

Figure 41 Compressor Speed Result Respect to Time

In Figure 41, during the start-up, when the compressor's valves are closed and no mass is flowing through the machine, the rotor will accelerate at the same rate as the motor. When the valves open, point A, the rotor will slightly decelerate to compensate the increased load on the compressor. At point B, the system regulator will start to limit the compressor mass flow rate and controlling the acceleration rate of the motor. At point C, the motor reaches its maximum speed and keeps it almost constant until the desired pressure ratio is achieved, which is indicated by point D.

5.1.4 Mass Flow Rate

The mass flow rate behaviour is closely related to speed; they both are dependent on the compressor's characteristics, and the output pressure required by the system, as can be seen on Figure 42. During start-up, the mass flow rate is zero, then, when the valves open at 50% of the nominal speed, it instantaneously jumps to the value that matches the current speed and pressure ratio. This is represented by point A on Figure 42. The instantaneous jump occurs, because there is no delay in the model to set the time that takes to open the inlet valves. At point B on Figure 42, the mass flow rate reaches its limit for that operation point, and the system regulator will control its increment rate. In practice this is done by bleeding valves, throttling inlet valves, and controlling the compressor's speed. At point C, the system reaches its maximum speed which is kept almost constant, the mass flow rate is then decreased due to the increase in backpressure from the cavern. From the results, it can be seen that it takes 296 seconds to increase the pressure of a cavern of 3000 m^3 by 3bar, using an axial compressor that has a nominal mass flow rate of 55 kg/s.

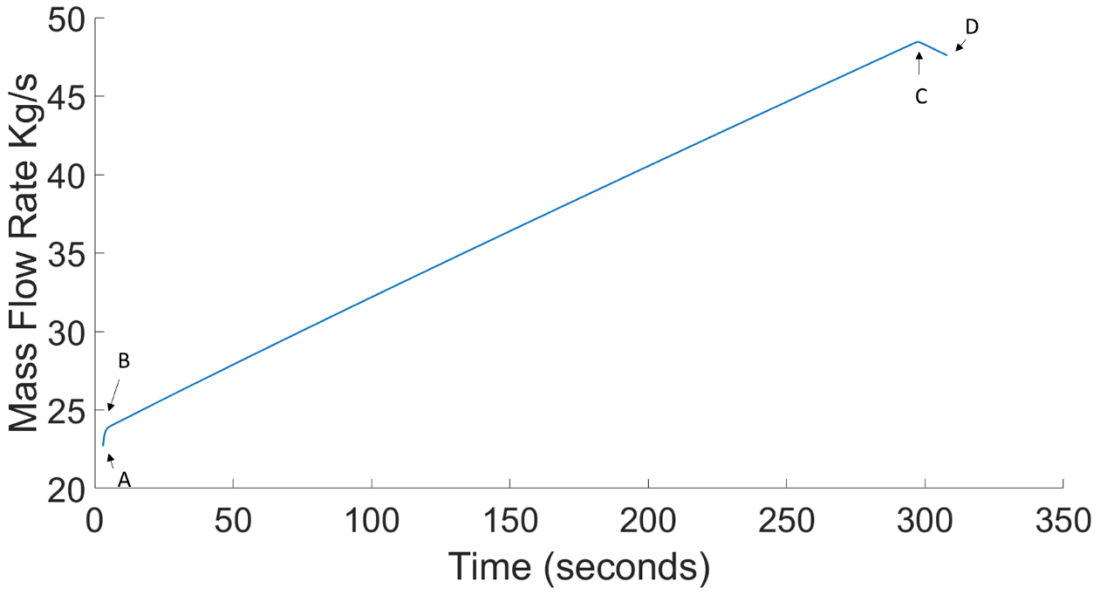

Figure 42 Compressor Mass Flow Rate Result Respect to Time

5.1.5 Compressor's Efficiency

The efficiency results are heavily influenced by the mass flow rate and the speed, as expected from the map. The highest efficiency of 72.95% as shown by point E on Figure 43, is reached at approximately 92% of the maximum speed at a mass flow rate of 44 kg/s. The total variation of efficiency, from lowest to highest point is 5%, which shows a partially stable operation. This is achieved because of the regulating system, which tries to achieve a high efficiency. However, this regulating system is not completely optimized, especially at low mass flow rates around 22 to 40 kg/s, as can be seen in Figure 44; that is one of the reasons why the efficiency results are on the lower side. The average efficiency operation of the compression cycle is 71.09% and this can be increased by incorporating an optimized controlling system. The other reason behind having low efficiencies is due to the map scaling method. In this method, the map is scaled keeping the same number of stages, which increases the work required per stage, also known as stage loading; this reduces the isentropic efficiency of the machine, therefore contributing to the low efficiency results [49], [64].

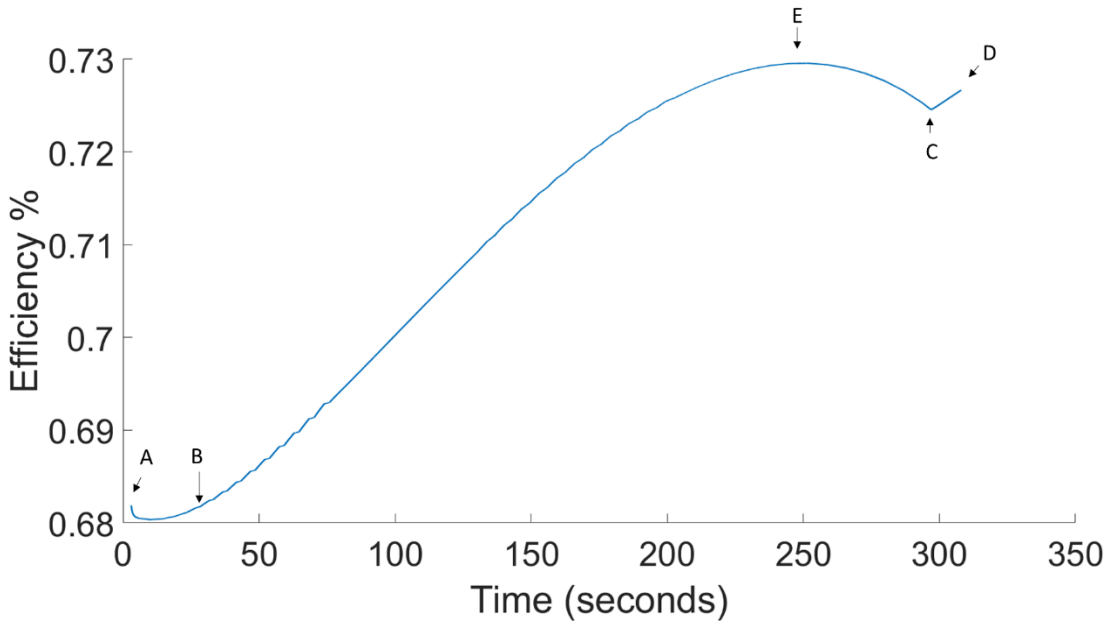

Figure 43 Compressor Efficiency Result Respect to Time

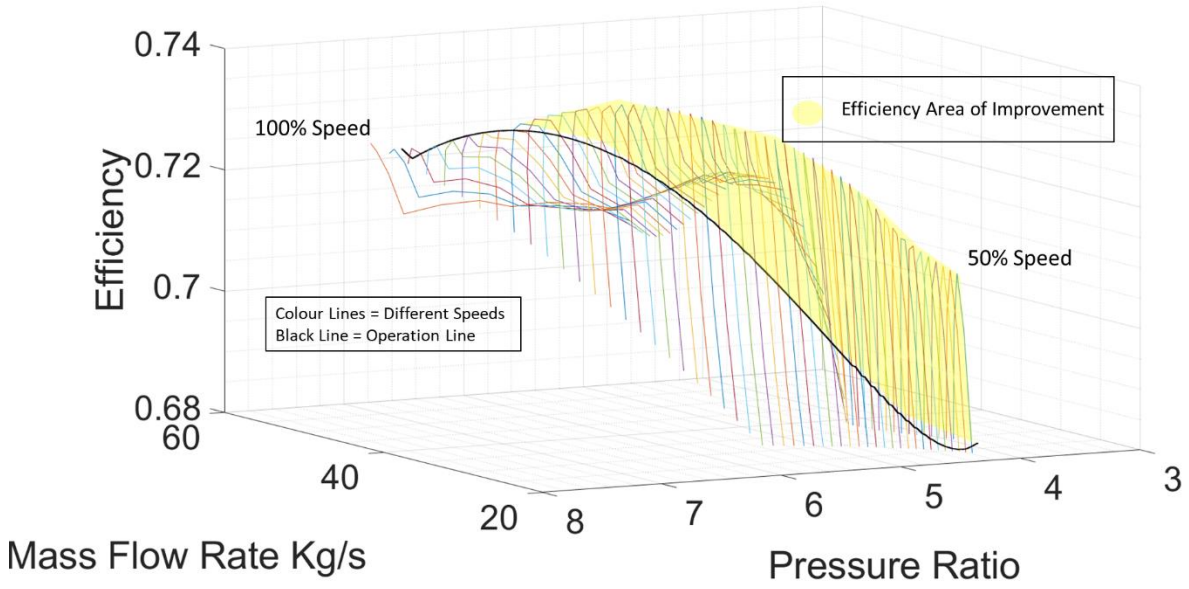

Figure 44 Efficiency Result in Performance Map 3D

5.1.6 Stored Energy

The specific work rate done by the compressor on the air per unit time is obtained by using equation 43 below

$$\dot{w} = \dot{m}(h_{out} - h_{in}) \tag{43}$$

Where $\dot{m}$ is the mass flow rate in kg/s, h_{out} is the enthalpy of the air coming out of the compressor and h_{in} is the enthalpy of the air just before entering the compressor. Assuming the air is stored as it comes out of the compressor, with no losses and no temperature changes, the energy stored can be obtained by equation

$$\text{Ideal stored energy} = \int_{t=0}^{t=n} \dot{m}(h_{out} - h_{in})dt \tag{44}$$

Using these equations on the simulation results, the stored energy with respect to time is obtained, Figure 45 shows this.

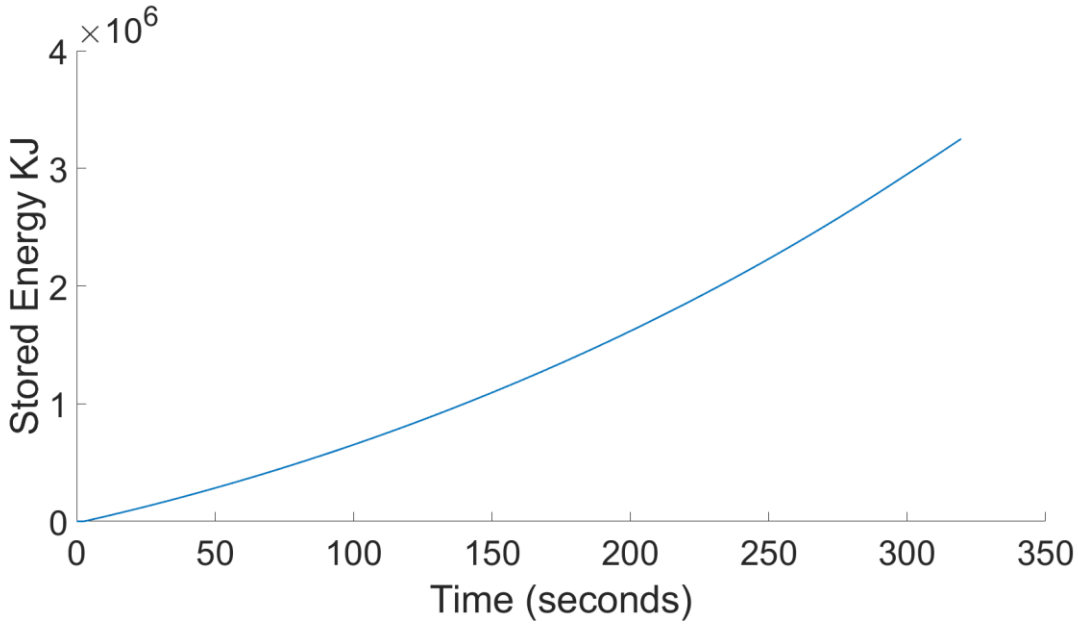

Figure 45 Ideal Energy Stored in Cavern

The ideal stored energy in the cavern, after increasing its pressure from 4 to 7 bar is 3.2507e6 KJ.

5.1.7 Cavern Size Change

As mentioned in section 5.1.1, the cavern size chosen for the simulation is 100 times smaller than Huntorf's cavern; this is done in order to make the simulation time shorter. Another simulation is run, with a cavern 10 times larger than the one used in the original run. A few results obtained from it are shown in Figure 46 and Figure 47.

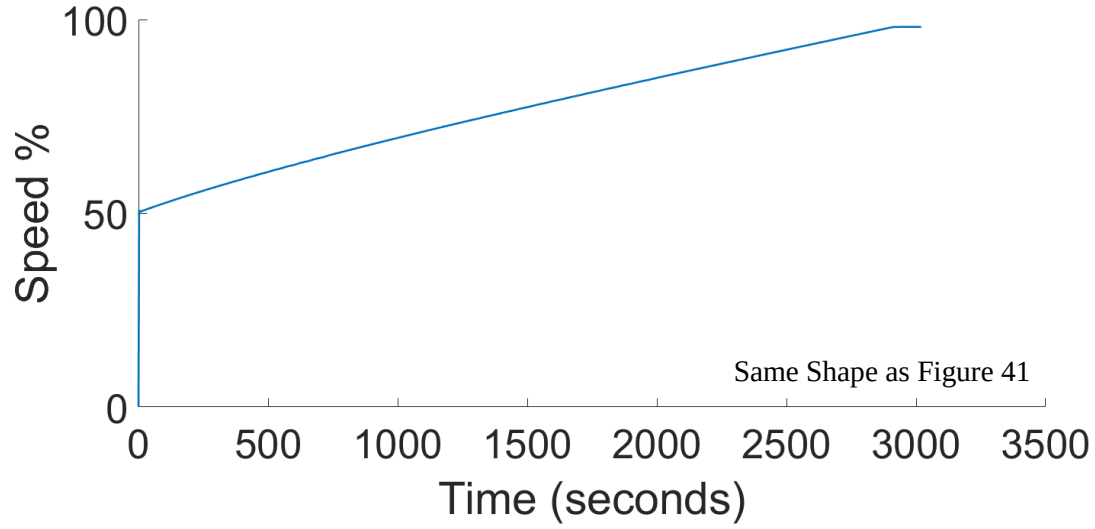

Figure 46 Compressor Rotor Speed Result of Second Simulation, Cavern 100 Times Larger

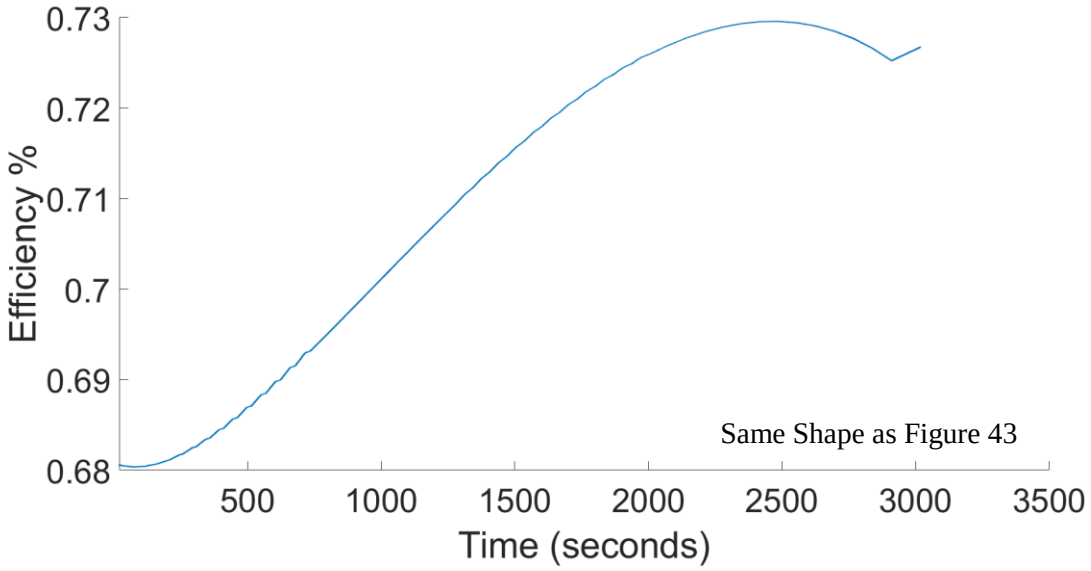

Figure 47 Compressor Efficiency Result of Second Simulation, Cavern 100 Times Larger

As seen on the two graphs above, the results obtained by using a cavern 10 times larger have the same pattern as the original ones. The only difference between them is that the time span difference between both cycles is directly proportional to the caverns' size difference.

The compressor simulation shows expected results. It stays inside the operation range given by the maps and works at part load most of the time. The time it takes the compressor to reach the valve opening speed depends on the characteristics of the compressor, the nominal power of the motor, and the size of the pressure container. For this simulation, the cavern size is one hundred times smaller than the Huntorf cavern, and the chosen mass flow rate is half of the nominal mass flow rate of the Huntorf plant. This is done in order to achieve a shorter simulation time without affecting the fidelity of the results. In the section that follows, the results obtained from the turbine simulation are presented.

5.2 Turbine Simulation

The turbine model is simpler than the compressor model, it has a constant pressure ratio due to the regulator valve located upstream from the turbine, and the outlet pressure is assumed to be ambient. The main goals of modelling the turbine is to see how it reacts to changes to the load connected to it; the time it takes during start-up to reach the required operation point, as well as how the efficiency of the machine changes during this time. There are two versions of the simulation, one where the load starts at zero and after 10 seconds it increases to its nominal value and remains steady. In the second version, the load is now varied, and it increases and decreases slightly beyond nominal conditions. In both versions, the turbine starter is only compressed air, and no electric motor is used throughout the simulation. This type of starting method was chosen because it fits the CAES' conditions and operation [82]. The initial data required for the simulation is show on Table 5, data marked with the symbol * is taken from [68] because it is based on the Huntorf CAES plant.

Table 5 Turbine Simulation Data

Parameter	Value
Ambient Pressure	101 Kpa
Pressure Ratio	2
Inlet Temperature	1573 K°
Nominal Speed	3600 Rpm *
Nominal Load	167 MW
System Inertia	5070 Kg m^2 *
System Friction Factor	0.02 *
Nominal Mass Flow Rate	400 Kg/s *

* Data obtained from [68]

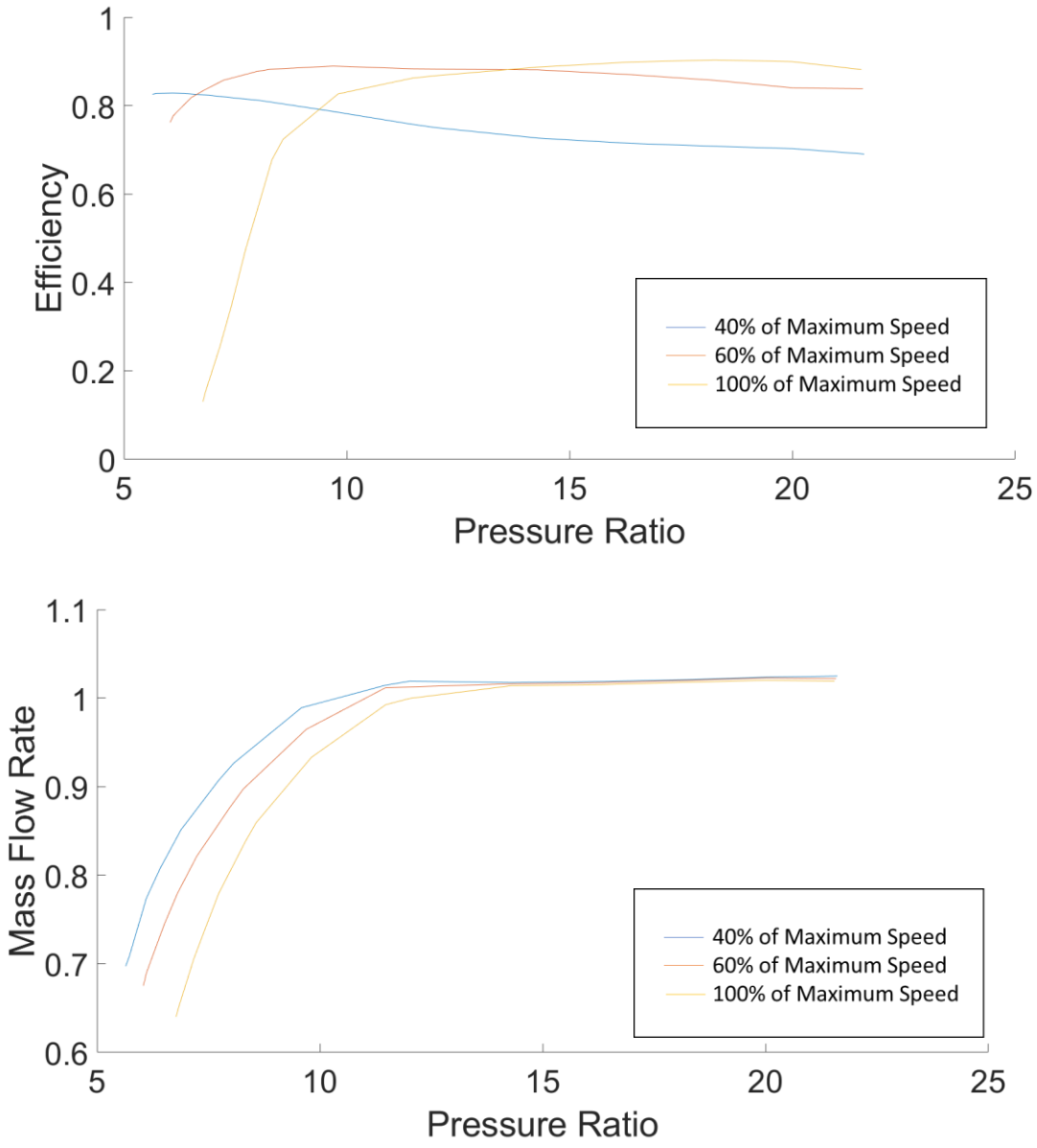

Figure 48 Turbine Maps

5.2.1 Simulation Time Step

The time step used for both turbine simulations is the continuous time step, because the simulations run in less than 3 minutes with good detail.

5.2.2 Steady Nominal Conditions – Angular Speed

During the steady nominal conditions simulation, the turbine begins to spin from rest. Then, after 10 seconds, it is connected to the load, as illustrated by point A below in Figure 49. The results obtained from this simulation show that this turbine will need 778 seconds to reach its nominal point, as seen on point B of Figure 49.

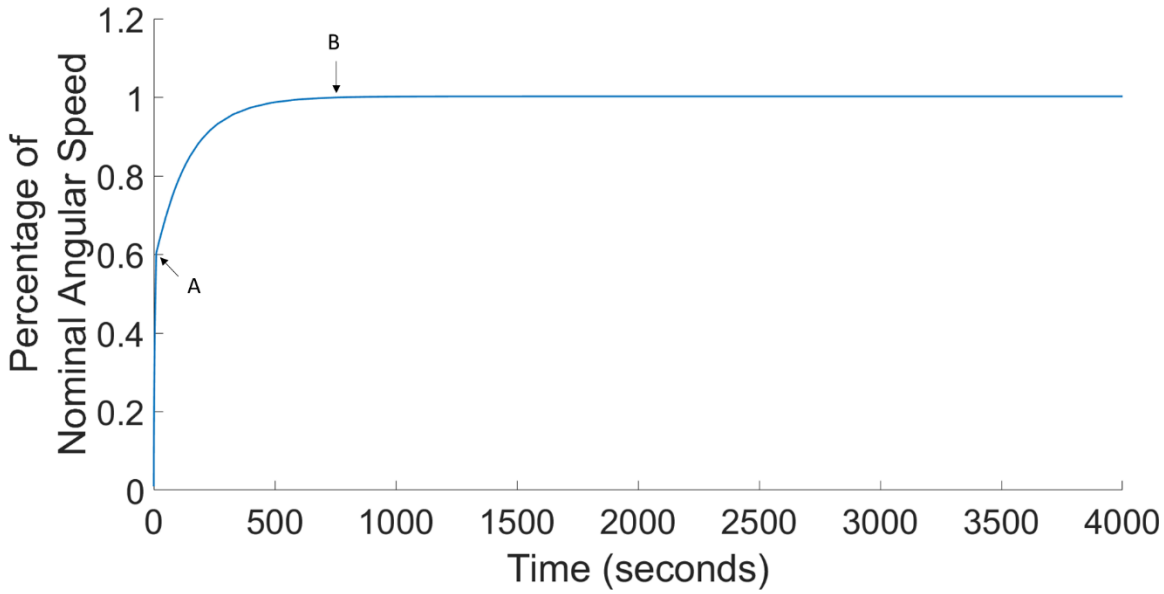

Figure 49 Turbine Angular Speed Result, Steady Nominal Conditions

5.2.2.1 Influence of the System's Moment of Inertia

Upon observing the result obtained in Figure 49, another simulation is run. This time, with a smaller system moment of inertia; this is done to see how much having a lighter turbine and lighter electric generator would affect the start up time. This test is done by reducing the turbine moment of inertia by 10% decremented steps, from 100 to 50%. The results are seen in Figure 50. It can be seen there, that the time it takes the system to reach the nominal speed varies linearly with the moment of inertia of the system. This result is going to play a key role when choosing the machinery for a CAES project according to the services planned to provide.

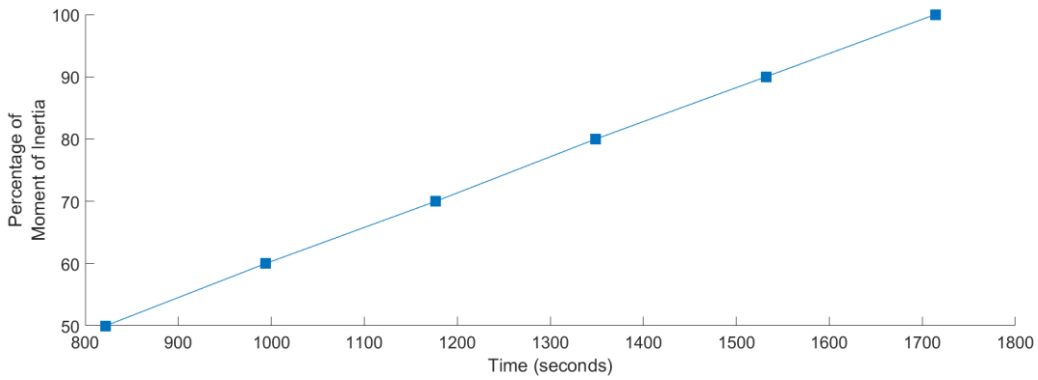

Figure 50 Effect of Moment of Inertia on Turbine Start-up Time

5.2.3 Steady Nominal Conditions – Mass Flow Rate

The mass flow rate begins initially at its maximum value because it needs a huge amount of power to start moving the machine. Then, as the speed increases, the mass flow rate decreases until it reaches a steady value; which is approximately 94% of its maximum value. This is expected since on the turbine operation map, as seen in Figure 48 , the mass flow rate has this value at the selected pressure ratio of 12.

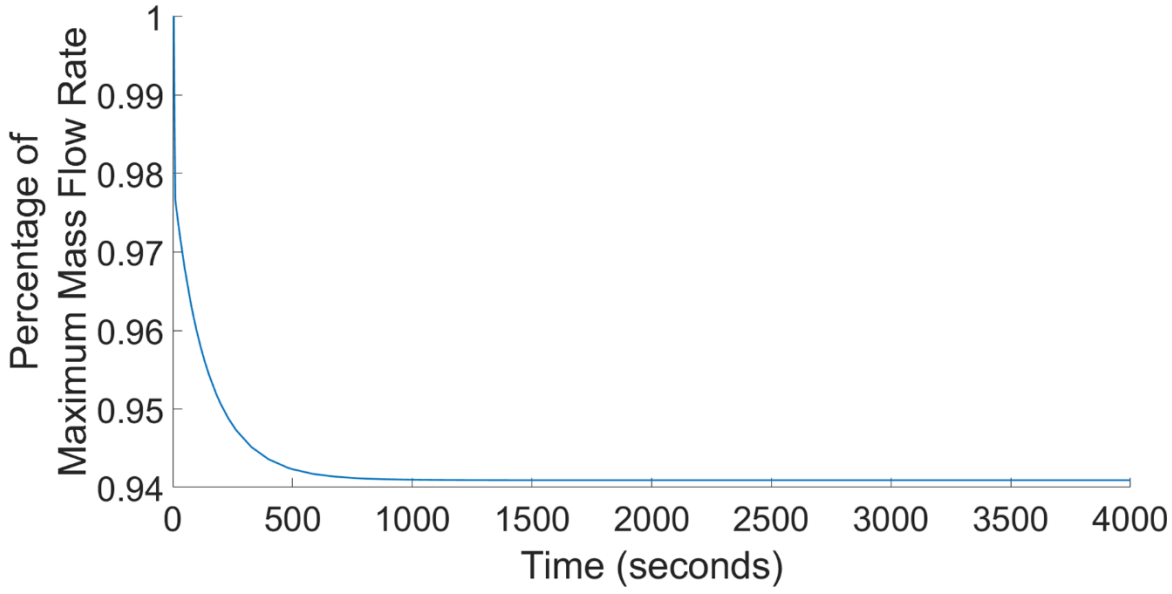

Figure 51 Turbine Mass Flow Rate Result, Steady Nominal Conditions

5.2.4 Steady Nominal Conditions – Efficiency

According to the efficiency performance map, the efficiency of the turbine reaches its optimum point when the pressure ratio is close to 20, at an angular speed of about 100%. This is represented as point A1 on Figure 52. When the selected pressure ratio is 12, the maximum efficiency point on the map occurs when the angular speed is at 60%, as show by point B1 on Figure 52. However, at values between 60 to 99% it has efficiencies higher than the one achieved at 100% speed, also seen at point B1 on Figure 52. This explains the results obtained from the simulation, which are shown on Figure 53. At speeds below 60%, the simulation shows efficiency values close to 70-80%. Then, as the machine keeps accelerating, it has a peak efficiency of 87.8% at a speed of 70%, as indicated by point C on Figure 53. It then decreases and reaches a steady state efficiency value of approximately 83%, at nominal conditions.

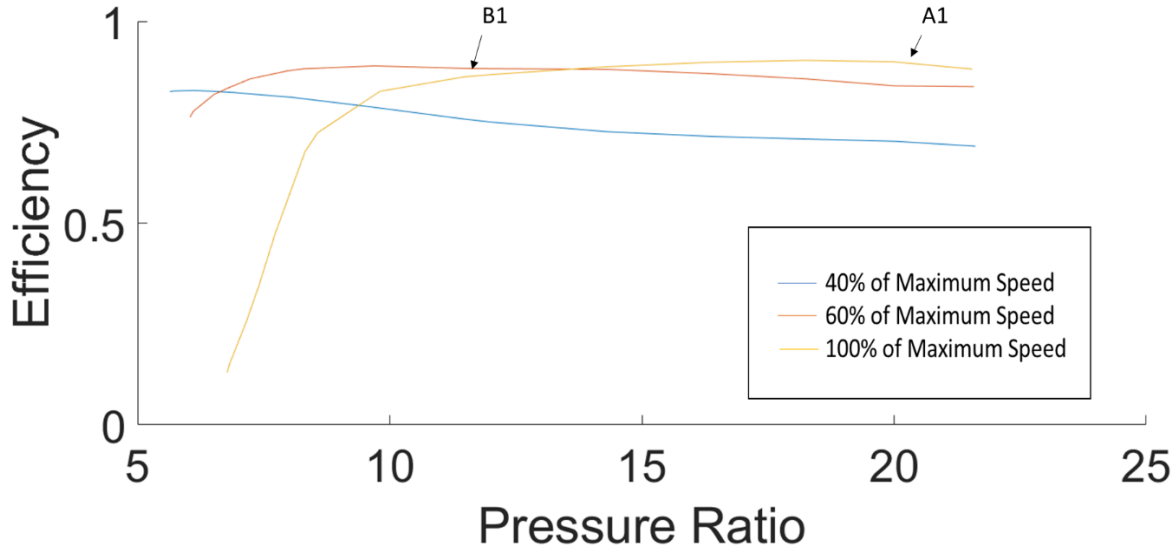

Figure 52 Turbine Performance Map, from [57]

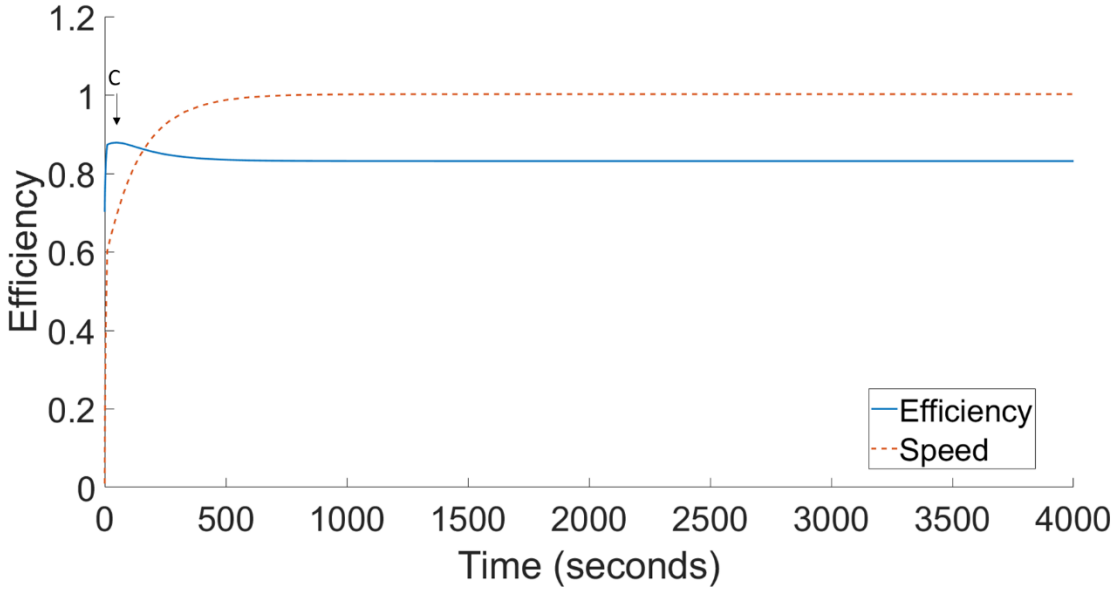

Figure 53 Turbine Efficiency and Angular Speed Results, Steady Nominal Conditions

5.2.5 Variable Conditions - Load

The second part of the turbine simulation has a variable load connected to the turbine; the purpose of this is to study how the turbine reacts to load variation and how much time does it take to regain stability. The selected variable load starts at zero and then increases and decreases up to 20 % away from the nominal point, which can occur in real power generation turbine engines. The load variation with respect to time, for this simulation is shown on Figure 54.

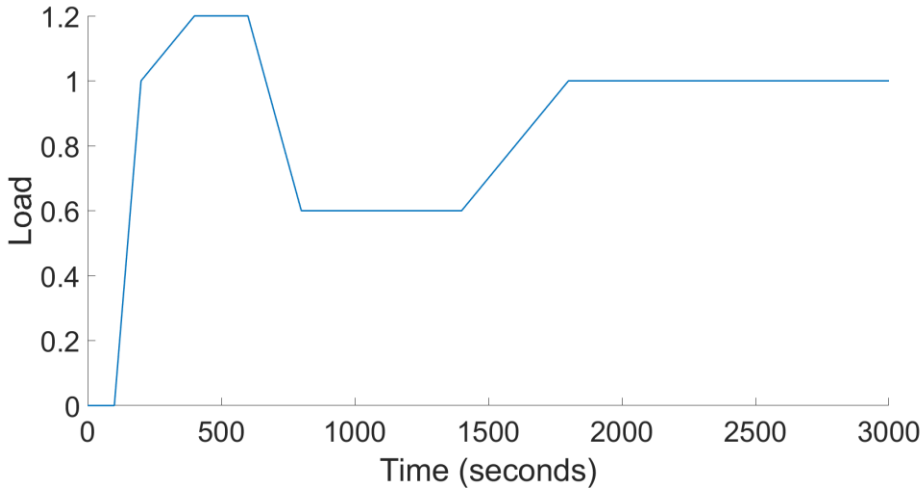

Figure 54 Turbine Load Arbitrary Simulated Signal

5.2.6 Variable Conditions – Angular Speed

The angular speed is increasing in the beginning of the simulation and the load is 0%, as can be seen from points A to B in Figure 55. When the load reaches 50% the turbine stops accelerating, this is shown by points CL and CS. When the load reaches 82%, the turbine starts decelerating, this is represented by points DL and DS. Then, when the load is higher than nominal conditions the speed decreases, as seen from point GL to HL, and also from point GS to HS. When the load is lower than nominal conditions the speed will increase, as is reflected on sections IL and IS. This typically happens in power plants and is what provokes the need of frequency regulation services. The load and the speed have an inverse relationship. When the load is higher than nominal conditions the speed will decelerate, and when the load is lower than nominal conditions the turbine will accelerate. When the load is at nominal conditions the speed will remain constant, and provide the required power and frequency.

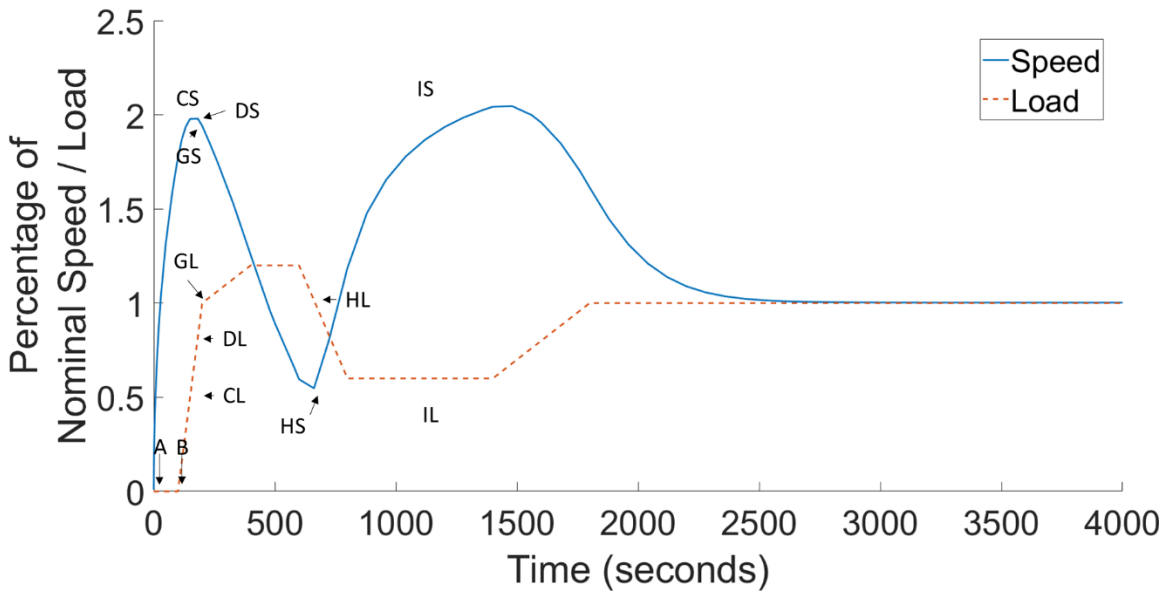

Figure 55 Turbine Angular Speed and Load Result, Variable Conditions Simulation

5.2.7 Variable Conditions – Mass Flow Rate

The mass flow rate, similar to the nominal conditions test, starts at the maximum point and decreases below its nominal value as the turbine starts accelerating. Initially, the load is 0%; this is shown on the graph from point AL to BL on Figure 56. When the load reaches 50% of its nominal amount, this is represented by point CL; the turbine stops accelerating and remains steady for a short amount of time, as can be seen at section CS. When the load reaches 80%, this is marked by point DL, the

turbine starts decelerating, and the mass flow rate starts increasing, as seen on points DS and DM. As the load stays higher than the nominal condition, the speed will continue decreasing, and the mass flow rate will keep increasing until it reaches the choking condition, as marked by point EM. As the load decreases, the mass flow rate will also decrease even if the load goes below the nominal point, as can be seen from point EM to FM, and EL to FL. When the load starts increasing the mass flow rate will follow. The load and the mass flow are directly proportional because the mass flow gives the power to the turbine to reach the required load. The delay in the mass flow rate adjustment is attributed to the moment of inertia of the system.

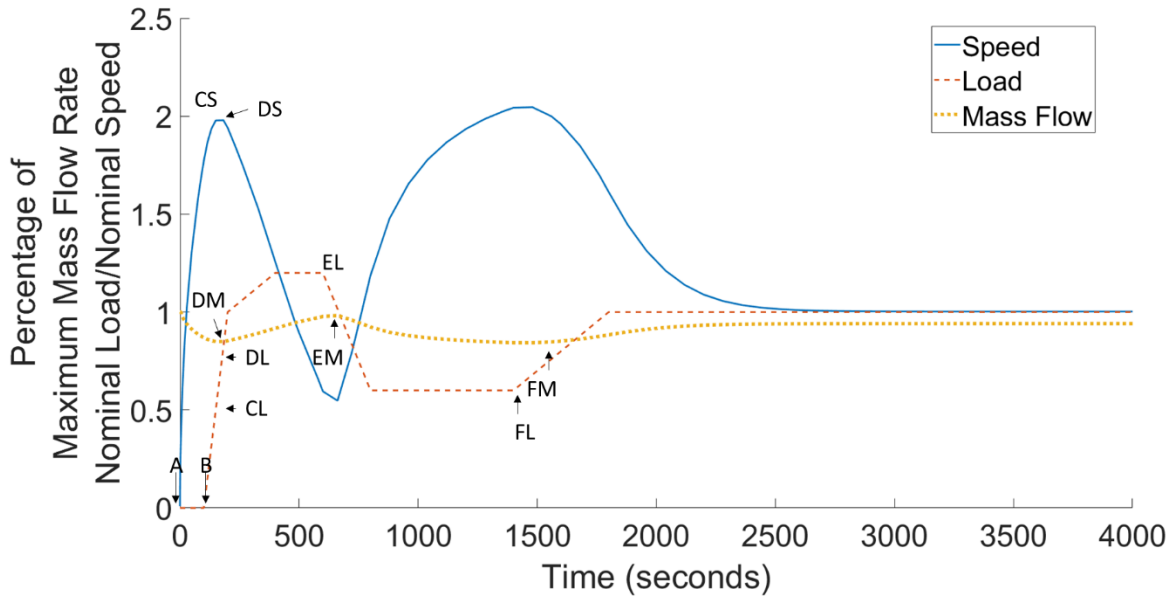

Figure 56 Turbine Mass Flow Rate Result, Variable Conditions Simulation

5.2.8 Variable Conditions – Efficiency

Similar to what was observed during steady state conditions, when the angular speed increases beyond 80%, the machine's efficiency decreases, as seen on point A in Figure 57. Then, when the speed starts decreasing, and getting closer to the 80% of the nominal value, the efficiency increases; as can be seen at point B and C in Figure 57. When the load decreases and the turbine accelerates to values higher than nominal, the efficiency decreases as dictated by the performance map. This can be seen at point D on Figure 57.

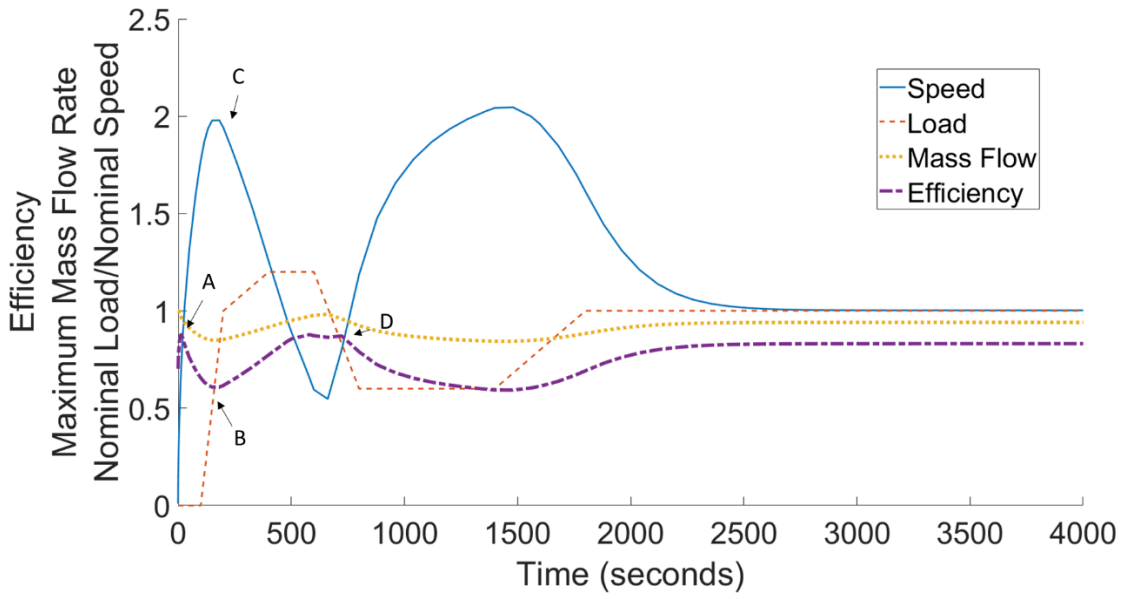

Figure 57 Turbine Efficiency Result, Variable Conditions Simulation

5.2.9 Round Trip Efficiency

Upon charging a 3000 m^3 cavern with compressed air and then expanding that air in the turbine; an electrical power input of 4478.1 KJ is used and a shaft power output of 2471.1 KJ is obtained, giving an overall efficiency of 55%. This result is higher than the 41% efficiency obtained in the Huntorf plant [80]. This occurs because the level of detail of the developed models does not take into account the losses from the cavern as well as and the generator.

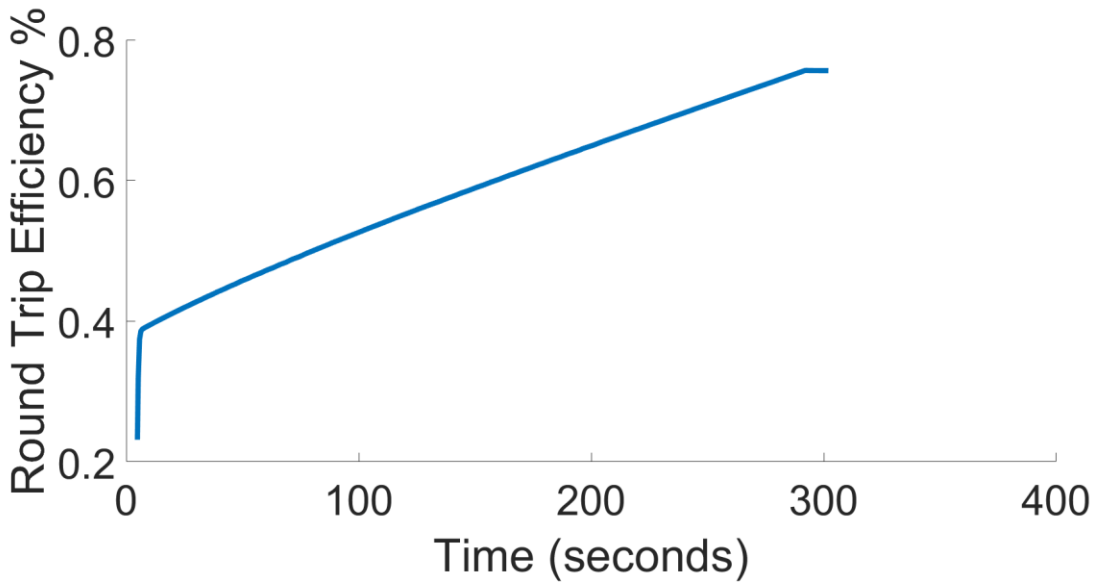

Figure 58 Round Trip Efficiency

This chapter has shown the results obtained from both simulations. At this time, these results cannot be validated because there is no experimental data to compare the results against. However, the results show a close resemblance to the turbomachinery maps, which is what it is expected. The times obtained from the turbomachine simulation results are limited to the amount of real data that is available; therefore, they need to be interpreted cautiously. The modelled compressor and turbine are not the same as the ones being used in the Huntorf plant. The maps of those machines are not available in the literature. Nonetheless, when using these models in conjunction with maps of the machines to be modelled, the time results will always be representative. The models developed in this work will aid a CAES plant engineer to design a general or specific CAES plant, and to generate specifications for the required turbomachinery, as well as for other components within the plant such as the cavern and its size.

Chapter 6
Conclusion and Recommendations

6.1 Conclusions

Two axial turbomachinery models for CAES systems have been created and explained in this work, one for a compressor and one for a turbine. The models use turbomachinery maps to capture the complex fluid phenomena occurring in the machines. The novelty of the models is that they consider the compressor driver transients, as well as the inertias present in the process, which are reflected significantly in the turbine simulation results. They can be used in efficiency tests, control strategy design, plant operational-mode range selection, among others. From the simulations run, the key results that were obtained are outlined below:

- It takes 296 seconds to increase the pressure of a cavern of 3000 m^3 from 422.18 Kpa to 747.4 Kpa using an axial compressor that has a nominal mass flow rate of 55 kg/s.
- During the charging process where the cavern pressure increases from 422.18 Kpa to 747.4 Kpa, the average efficiency of the compressor is 71. %; and this can be increased by incorporating an optimized controlling system
- For the turbine, when there is a difference between the nominal and the current loads, the machine will accelerate as long as the current load is lower than the nominal; and it will decelerate as long as the current load is higher than the nominal load.
- For a 167 MW turbine, with a design speed of 17000 rpm, with a nominal mass flow rate of 400 kg/s, it will take the turbine 778 seconds to reach its nominal speed.
- For this simulation with the afore mentioned conditions, the overall efficiency obtained is 55%. This result is higher than the 41% efficiency obtained in the Huntorf plant, because the developed models do not consider the losses from the cavern as well as and the generator.
- The relationship between the turbine moment of inertia and the time taken for the turbine to achieve nominal power is linear; which means that lighter turbines and lighter generators will reach their nominal speeds faster.

The developed models have the following additional characteristics:

- The models are relatively simple and fast as compared to computational fluid dynamics models; thus, a complex control system can be added to them for analysis purposes.

- The models work in SIMULINK®, which is one of the most common tools used for electrical and electronic design, therefore they can be easily used in power grid connection analyses.
- The developed models can represent the behavior of any axial and centrifugal turbomachine, provided that there is a map associated with it.
- The turbine model is flexible enough to run under a variable inlet pressure scenario, this can be done by adding a cavern model to simulate the phenomena inside the cavern.

6.2 Limitations

Along with its benefits, the model also has some limitations. The time results obtained from the simulations are initial approximations; however, the model is flexible enough to accommodate specific cases. If a specific case wants to be replicated, for example the Huntorf CAES plant, real values for the plant parameters must be provided, e.g., motor's initial values, exact nominal conditions, operational mode, machines' arrangement, etc. The regulation system for this work is designed to keep the operating points within the turbomachinery map limits, i.e., the regulation system does not try to achieve the highest efficiency, or the fastest of times; a different regulation strategy should be applied if any other scenario is to be studied.

6.2.1 Huntorf Compressor Train

The Huntorf CAES plant contains an axial and centrifugal compressor connected in series [83]. The developed model, can simulate the axial compressor with variable speed. For the Huntorf plant, there is little to no published information regarding the nominal pressure ratios of the machines, nor is there information published on the control and operational mode, i.e. variable geometry or variable speed. The model methodology proposed in this work can be used to simulate a variable speed centrifugal compressor used in a CAES plant, provided the corresponding compressor map. In this way, the entire compressor train of a CAES plant with similar configuration as the Huntorf plant can be simulated, as part of future work.

6.2.2 Efficiency

The efficiency results obtained from the compressor simulation, reflect the performance of a variable speed axial compressor. However, these efficiency results represent only the losses that occur inside

the machine, not taking into account the inlet throttling losses or bleed losses produced during the operation.

6.2.3 Variable Geometry

If a compressor with variable guide vanes and constant speed is desired to be modeled, there are a few considerations to consider. If a variable compressor guide vane map is available, the simulation methodology would require a set of initial guesses for the entire starting process until the desired operating speed is achieved. Then, a governor system is needed to control the speed. The best scenario will be to obtain a map that contains on it, how the speed varies with the orientation of the guide vanes. Unfortunately, such maps are not commonly created by machine manufacturers, and hence may have to be experimentally obtained. Some publications mention ways to model the effects of variable guide vanes, also known as variable geometry. Some of them model this behaviour in a generalized way, either using an s-domain transfer function, or through experimental tests [36], [84], [85]. Other works, are based on the assumption that each stage of a machine has identical stage characteristics, and utilize long iteration methods to create a compressor map for each valve position [39], [47], [86].

6.3 Recommendations

Although the simulation results fit the expected performance of a turbomachine well, it is recommended that the model is validated with physical measurements and data. This can be done in a laboratory with a micro turbine and compressor along with a pneumatic or hydraulic system.

To further evolve this model into a specific scenario, the following next steps are recommended to build upon this work:

- To add a generator model to the turbine to simulate synchronous or asynchronous operation modes.
- To experiment with other types of motors for the compressor to find the best fit for a particular scenario.
- To add the time delays that reflect the valve opening-closing operation.
- To add the time delays that reflect the initial procedure required for the turbine, e.g., warmup time, purge time, among others.

- To add bleed losses and throttling losses of the system.
- To add the effects of variable machine geometry for performance, as well as operation of the system.
- To create a methodology to develop custom turbomachine maps, where parameters such as pressure ratios and number of stages can easily be varied; and their effect on the map can be studied.
- To add a centrifugal compressor to the model, in order to replicate a CAES plant having a configuration similar to Huntorf.
- To incorporate a control strategy that optimizes the efficiency of the system.

References

[1] F. Sioshansi, “Prospects for Renewable Energy,” in *Energy, Sustainability and the Environment - Technology, Incentives, Behavior*, Elsevier, 2011, p. 367.

[2] F. Sioshansi, “Can We Have Our Cake and Eat It Too?,” in *Energy, Sustainability and the Environment - Technology, Incentives, Behavior*, Elsevier, 2011, p. xxviii.

[3] T. M. Letcher, “Hydropower and Sustainability,” in *Future Energy - Improved, Sustainable and Clean Options for Our Planet*, Elsevier, 2008.

[4] P. Breeze, *Power Generation Technologies*, 2nd ed. Elsevier, 2014.

[5] “Discover Renewable Energy Technology with Compressed Air Energy Storage,” *Pacific Gas and Electric Company*, 2017. [Online]. Available: https://www.pge.com/en_US/about-pge/environment/what-we-are-doing/compressed-air-energy-storage/compressed-air-energy-storage.page.

[6] R. Leithner and L. Nielsen, “CHAPTER 13 An introduction to the compressed air energy storage,” in *Computational Models for CO2 Geo-sequestration & Compressed Air Energy Storage*, CRC Press, 2014, pp. 423–434.

[7] J. E. Mason and C. L. Archer, “Baseload Electricity from Wind Via Compressed Air Energy Storage (CAES),” *Renew. Sustain. Energy Rev.*, vol. 16, no. 2, pp. 1099–1109, 2012.

[8] P. Zhao, L. Gao, J. Wang, and Y. Dai, “Energy efficiency Analysis and Off-design Analysis of Two Different Discharge Modes for Compressed Air Energy Storage System Using Axial Turbines,” *Renew. Energy*, vol. 85, pp. 1164–1177, 2016.

[9] T. Das, V. Krishnan, Y. Gu, and J. D. McCalley, “Compressed air energy storage: State space modeling and performance analysis,” *2011 IEEE Power Energy Soc. Gen. Meet.*, pp. 1–8, 2011.

[10] H. Safaei and M. J. Aziz, “Thermodynamic analysis of a compressed air energy storage facility exporting compression heat to an external heat load,” 2014, pp. 1–10.

[11] D. Wolf, *Methods for Design and Application of Adiabatic Compressed Air Energy Storage Based on Dynamic Modeling*, vol. PhD, no. 65. 2010.

[12] R. Kushnir, A. Dayan, and A. Ullmann, “Temperature and Pressure Variations within Compressed Air Energy Storage Caverns,” *Int. J. Heat Mass Transf.*, vol. 55, no. 21–22, pp. 5616–5630, 2012.

[13] M. Raju and S. Kumar Khaitan, “Modeling and Simulation of Compressed Air Storage in Caverns: A Case Study of the Huntorf plant,” *Appl. Energy*, vol. 89, no. 1, pp. 474–481, 2012.

[14] R. Kushnir, A. Ullmann, and A. Dayan, “Thermodynamic and hydrodynamic response of compressed air energy storage reservoirs: A review,” *Rev. Chem. Eng.*, vol. 28, no. 2–3, pp. 123–148, 2012.

[15] C. Xia, Y. Zhou, S. Zhou, P. Zhang, and F. Wang, “A simplified and unified analytical solution for temperature and pressure variations in compressed air energy storage caverns,” *Renew. Energy*, vol. 74, pp. 718–726, 2015.

[16] G. Grazzini and A. Milazzo, “Exergy Analysis of a Caes With Thermal Energy Storage,” *Integr. Vlsi J.*, no. figure 1, 2015.

[17] G. Grazzini and A. Milazzo, “A thermodynamic analysis of multistage adiabatic CAES,” *Proc. IEEE*, vol. 100, no. 2, pp. 461–472, 2012.

[18] G. Grazzini and A. Milazzo, “Thermodynamic analysis of CAES/TES systems for renewable energy plants,” *Renew. Energy*, vol. 33, no. 9, pp. 1998–2006, 2008.

[19] N. M. Jubeh and Y. S. H. Najjar, “Green solution for Power Generation by Adoption of Adiabatic CAES System,” *Appl. Therm. Eng.*, vol. 44, pp. 85–89, 2012.

[20] A. Sciacovelli *et al.*, “Dynamic simulation of Adiabatic Compressed Air Energy Storage (A-CAES) plant with integrated thermal storage – Link between components performance and plant performance,” *Appl. Energy*, vol. 185, pp. 16–28, 2017.

[21] Z. Guo, G. Deng, Y. Fan, and G. Chen, “Performance optimization of adiabatic compressed air energy storage with ejector technology,” *Appl. Therm. Eng.*, vol. 94, pp. 193–197, 2016.

[22] N. Hartmann, O. Vöhringer, C. Kruck, and L. Eltrop, “Simulation and analysis of different adiabatic Compressed Air Energy Storage plant configurations,” *Appl. Energy*, vol. 93, pp. 541–548, 2012.

[23] E. Barbour, D. Mignard, Y. Ding, and Y. Li, “Adiabatic Compressed Air Energy Storage with packed bed thermal energy storage,” *Appl. Energy*, vol. 155, pp. 804–815, 2015.

[24] D. S. Rubio, “Isothermal Efficiency of Liquid Piston Compressors Employed in Compressed Air Energy Storage Systems,” pp. 1–8, 2016.

[25] X. Luo *et al.*, “Modelling Study, Efficiency Analysis and Optimisation of Large-scale Adiabatic Compressed Air Energy Storage Systems with Low-Temperature Thermal Storage,” *Appl. Energy*, vol. 162, pp. 589–600, 2016.

[26] a. Kere, V. Goetz, X. Py, R. Olives, N. Sadiki, and E. Mercier, “Dynamic Behavior of a Sensible-heat based Thermal Energy Storage,” *Energy Procedia*, vol. 49, pp. 830–839, 2014.

[27] Y. Zhang, K. Yang, X. Li, and J. Xu, “The Thermodynamic Effect of Thermal Energy Storage on Compressed Air Energy Storage System,” *Renew. Energy*, vol. 50, pp. 227–235, 2013.

[28] K. Yang, Y. Zhang, X. Li, and J. Xu, “Theoretical evaluation on the impact of heat exchanger in Advanced Adiabatic Compressed Air Energy Storage system,” *Energy Convers. Manag.*, vol. 86, pp. 1031–1044, 2014.

[29] C. Prieto, R. Osuna, A. I. Fernández, and L. F. Cabeza, “Thermal storage in a MW scale. Molten salt solar thermal pilot facility: Plant description and commissioning experiences,” *Renew. Energy*, vol. 99, pp. 852–866, 2016.

[30] Y. Zhang, K. Yang, X. Li, and J. Xu, “Thermodynamic analysis of energy conversion and transfer in hybrid system consisting of wind turbine and advanced adiabatic compressed air energy storage,” *Energy*, vol. 77, pp. 460–477, 2014.

[31] S. Zunft, C. Jakiel, M. Koller, and C. Bullough, “Adiabatic Compressed Air Energy Storage for the Grid Integration of Wind Power,” *Sixth Int. Work. Large-Scale Integr. Wind Power tTransmission Networks Offshore Wind.*, no. October, pp. 26–28, 2006.

[32] D. Wolf, A. Kanngießer, M. Budt, and C. Doetsch, “Adiabatic Compressed Air Energy Storage co-located with wind energy-multifunctional storage commitment optimization for the German market using GOMES,” *Energy Syst.*, vol. 3, no. 2, pp. 181–208, 2012.

[33] W. I. Rowen, “Simplified Mathematical Representations of Heavy-Duty Gas Turbines,” *J. Eng. Power*, vol. 105, no. 83, p. 865, 1983.

[34] J. Mantzaris and C. Vournas, “Modelling and Stability of a Single-shaft Combined Cycle Power Plant,” *Int. J. Thermodyn.*, vol. 10, no. 2, pp. 71–78, 2007.

[35] H. E. Shalan, M. a M. Hassan, and a B. G. Bahgat, “Parameter Estimation and Dynamic Simulation of Gas Turbine Model in Combined Cycle Power Plants Based on Actual Operational Data,” *J. Am. Sci.*, vol. 7, no. 5, pp. 303–310, 2011.

[36] M. R. Bank Tavakoli, B. Vahidi, and W. Gawlik, “An Educational Guide to Extract the Parameters of Heavy Duty Gas Turbines Model in Dynamic Studies Based on Operational Data,” *IEEE Trans. Power Syst.*, vol. 24, no. 3, pp. 1366–1374, 2009.

[37] F. P. de Mello and D. J. Ahner, “Dynamic Models for Combined Cycle Plants in Power System Studies,” *IEEE Trans. Power Syst.*, vol. 9, no. 3, pp. 1698–1708, 1994.

[38] S. K. Yee, J. V. Milanovic, and F. M. Hughes, “Overview and Comparative Analysis of Gas Turbine Models for System Stability Studies,” *IEEE Trans. Power Syst.*, vol. 23, no. 1, pp. 108–118, 2008.

[39] J. H. Kim, T. W. Song, T. S. Kim, and S. T. Ro, “Model Development and Simulation of Transient Behavior of Heavy Duty Gas Turbines,” *J. Eng. Gas Turbines Power*, vol. 123, no. July 2001, p. 589, 2001.

[40] S. Kim, P. Pilidis, and J. Yin, “Gas Turbine Dynamic Simulation Using Simulink,” *Proc. SAE Power Syst. Conf.*, 2000.

[41] I. H. Ismail and F. S. Bhinder, “Simulation of Aircraft Gas Turbine Engines,” *J. Eng. Gas Turbines Power*, vol. 113, no. 1, pp. 95–99, 1991.

[42] Q. Z. Al-Hamdan and M. S. Y. Ebaid, “Modeling and Simulation of a Gas Turbine Engine for Power Generation,” *J. Eng. Gas Turbines Power*, vol. 128, no. 2, p. 302, 2006.

[43] R. Bettocchi and F. Fabbri, “Dynamic Modeling of Single-Shaft Industrial Gas Turbine,” in *International Gas Turbine and Aeroatgine Congress & Exhibition*, 1996, pp. 1–9.

[44] G. Crosa, F. Pittaluga, A. Trucco, F. Beltrami, A. Torelli, and F. Traverso, “Heavy-Duty Gas Turbine Plant Aerothermodynamic Simulation Using Simulink,” *J. Eng. Gas Turbines Power*, vol. 120, no. 3, p. 550, 1998.

[45] S. M. Camporeale, B. Fortunato, and M. Mastrovito, “A Modular Code for Real Time Dynamic Simulation of Gas Turbines in Simulink,” *J. Eng. Gas Turbines Power*, vol. 128, no. 3, p. 506, 2006.

[46] T. W. Song, T. S. Kim, J. H. Kim, and S. T. Ro, “Performance Prediction of Axial Flow Compressors Using Stage Characteristics and Simultaneous Calculation of Interstage Parameters,” *Proceedings of the IMechE*, vol. 215 Part A, no. 1. pp. 89–98, 2001.

[47] J. H. Kim, T. W. Song, T. S. Kim, and S. T. Ro, “Dynamic Simulation of Full Startup Procedure of Heavy-Duty Gas Turbines,” *J. Eng. Gas Turbines Power*, vol. 124, no. 3, p. 510, 2002.

[48] J. Kurzke, “How to Get Component Maps For Aircraft Gas Turbine Performance Calculations,” *Int. Gas Turbine Aerotngine Congr. Exhib.*, 1996.

[49] P. Walsh and P. Fletcher, *Gas Turbine Performance*, 2nd ed. Blackwell Science, 2004.

[50] I. S. A. Nelson, Z. S. Filipi, and D. N. Assanis, “The Use of Neural Nets for Matching Fixed or Variable Geometry Compressors With Diesel Engines,” *J. Eng. Gas Turbines Power*, vol. 125, no. 2, pp. 572–579, 2003.

[51] P. Moraal and I. Kolmanovsky, “Turbocharger Modeling for Automotive Control Applications,” no. 724, 1999.

[52] J. Jensen, A. Kristensen, S. Sorenson, N. Houbak, and E. Kendricks, “Mean Value Modeling of a Small Turbocharged Diesel Engine,” *SAE Int.*, 1991.

[53] M. Orkisz and S. Stawarz, “Modeling of Turbine Engine Axial-Flow Compressor,” *J. Propuls. Power*, vol. 16, no. 2, pp. 336–339, 2000.

[54] E. M. Greitzer, Z. S. Spakovszky, and I. A. Waitz, “Thermodynamics and Propulsion - Multistage Axial Compressors,” *Massachusets Institute of Technology*, 2007. [Online]. Available: http://web.mit.edu/16.unified/www/FALL/thermodynamics/notes/node92.html.

[55] S. L. Dixon and C. A. A. Hall, *Fluid Mechanics and Thermodynamics of Turbomachinery*, 6th ed. Oxford U.K.: Butterworth-Heinemann, 2010.

[56] I. Grant, *Basic Concepts in Turbomachinery*. Book Boon, 2009.

[57] H. Cohen, G. Rogers, and H. Saravanamuttoo, *Gas turbine Theory*, 4th ed. Longman Group Limited, 1996.

[58] R. Kurz and K. Brun, “Gas Turbine Performance - What Makes the Map,” *Proc. 29th Turbomach. Symp.*, pp. 246–262, 2000.

[59] D. G. Wilson and T. Korakianitis, “Energy Transfer in Turbomachines,” in *The Design of*

High-Efficiency Turbomachinery and Gas Turbines, vol. 392, no. March, The MIT Press, 1983, pp. 261–264.

[60] F. White, *Fluid Mechanics*, 7th ed. McGraw-Hill, 2009.

[61] C. Mataix and A. Arenas, *Turbomaquinas termicas: Turbinas de Vapor, Turbinas de Gas, Turbocompresores*. Dossat, 1988.

[62] R. H. Aungier, *Axial-Flow Compressors A Strategy for Aerodynamic Design and Analysis*. The American Society of Mechanical Engineers, 2003.

[63] T. Wright and P. Gerhart, "Dimensional Analysis and Similarity for Turbomachinery 2," in *Fluid Machinery*, 2nd ed., CRC Press, 2009, pp. 53–87.

[64] A. M. Y. Razak, *Industrial Gas Turbines Performance and Operability*. CRC Press, 2007.

[65] R. Vepa, *Dynamic Modeling, Simulation and Control of Energy Generation*. Springer, 2013.

[66] J. P. Veres, "Axial and centrifugal compressor mean line flow analysis method," *47th AIAA Aerosp. Sci. Meet. Incl. New Horizons Forum Aerosp. Expo. 5 - 8 January 2009, Orlando, Florida*, no. January, p. 92407, 2009.

[67] Y. A. Cengel and M. A. Boles, *Thermodynamics an Engineering Approach*, 5th ed. Boston, MA: McGraw-Hill Science/Engineering/Math, 2004.

[68] Y. Mazloum, H. Sayah, and M. Nemer, "Static and dynamic modeling comparison of an adiabatic compressed air energy storage system," *J. Energy Storage*, vol. 11, no. November 2016, pp. 178–190, 2015.

[69] Mathworks, "Asynchronous Machine," *R2017b Documentation, MATLAB*, 2006. .

[70] W. Ma, Y. Liu, M. Su, and N. Yu, "Multi-stage axial flow compressors characteristics estimation based on system identification," *Energy Convers. Manag.*, vol. 49, no. 2, pp. 143–150, 2008.

[71] J. Kurzke and C. Riegler, "A NEW COMPRESSOR MAP SCALING PROCEDURE FOR PRELIMINARY CONCEPTIONAL DESIGN OF GAS TURBINES," in *ASME IGTI Turbo Expo*, 2000, pp. 1–8.

[72] B. MacIssac and R. Langton, *Gas Turbine Propulsion Systems*. Wiley, 2011.

[73] M. Gholamrezaei and K. Ghorbanian, “Compressor map generation using a feed-forward neural network and rig data,” *Proc. Inst. Mech. Eng. Part A J. Power Energy*, vol. 224, no. 1, pp. 97–108, 2010.

[74] C. Kong, J. Ki, and M. Kang, “A new scaling method for component maps of gas turbine using system identification,” *J. Eng. Gas Turbines Power*, vol. 125, no. 4, p. 979, 2003.

[75] F. Sellers and J. Carl, “NASA TN D-7901 DYNGEN - A PROGRAM AND AND FOR CALCULATING PERFORMANCE ENGINE _ OF TURBOJET TRANSIENT Ohio and Daniele,” no. April 1975, 2018.

[76] E. Tsoutsanis, N. Meskin, M. Benammar, and K. Khorasani, “An Efficient Component Map Generation Method for Prediction of,” in *ASME Turbo Expo 2014: Turbine Technical Conference and Exposition*, 2014, pp. 1–12.

[77] M. Wentong, L. Yongwen, and S. Ming, “NEW SCALING METHOD FOR COMPRESSOR MAPS USING AVERAGE INFINITESIMAL STAGE,” *CHINESE J. Mech. Eng.*, vol. 20, pp. 24–28, 2007.

[78] R. Tirnovan, S. Giurgea, A. Miraoui, and M. Cirrincione, “Surrogate modelling of compressor characteristics for fuel-cell applications,” *Appl. Energy*, vol. 85, no. 5, pp. 394–403, 2008.

[79] B. Sankar, B. Shah, S. Thennavarajan, and V. Vanam, “On Gas Turbine Simulation Model Development,” no. October, pp. 1–17, 2013.

[80] A. G. Ter-Gazarian, “7.5.1 Huntorf,” in *Energy Storage for Power Systems (2nd Edition)*, Institution of Engineering and Technology, 2011.

[81] H. Asgari, M. Venturini, X. Chen, and R. Sainudiin, “Modeling and Simulation of the Transient Behavior of an Industrial Power Plant Gas Turbine,” *J. Eng. Gas Turbines Power*, vol. 136, no. 6, p. 61601, 2014.

[82] A. Beyene and T. Fredlund, “Comparative Analysis of Gas Turbine Engine Starting,” in *International Gas Turbine & Aeroengine Congress & Exhibition*, 1998.

[83] A. G. Ter-Gazarian, “Compressed air energy storage 7.1,” in *Energy Storage for Power Systems*, The Institution of Engineernig and Technology, 2011, pp. 99–120.

[84] W. I. Rowen, “Simplified Mathematical Representations of single-shaft gas turbines in mechanical drive services,” *Turbo Mach. Int.*, pp. 26–32, 1992.

[85] S. I. U. H. Gilani, A. T. Baheta, and C. Rangkuti, “Study the effect of variable vanes on performance of axial compressor for single shaft gas turbine cogeneration plant,” *ICEE 2009 - Proceeding 2009 3rd Int. Conf. Energy Environ. Adv. Towar. Glob. Sustain.*, no. December, pp. 40–44, 2009.

[86] D. E. Muir, H. I. H. Saravanamuttoo, and D. J. Marshall, “Health Monitoring of Variable Geometry Gas Turbines for the Canadian Navy,” *J. Eng. Gas Turbines Power*, vol. 111, no. 2, p. 244, 1989.

Appendix A
Flow Coefficient and Stage Loading

Flow Coefficient and Stage Loading are two important parameters which are used in gas turbine models; both appear in the stage characteristics curves, which are the main source of data for the performance maps In an axial flow machine, the flow coefficient ϕ is a non-dimensional factor that represents the ratio of axial-flow speed to blade speed, as seen in the next equation, obtained from [46] .

$$\phi = \frac{C_x}{U} \tag{45}$$

Where C_x is the axial velocity and U is the blade speed. For a fixed geometry and fixed blade speed, the flow coefficient will increase as the mass flow rate increases [55]. Low values of flow coefficient represent highly staggered blades; for the opposite is true for high values of flow coefficient. The stage loading coefficient ψ is the ratio of stagnation enthalpy change of a stage to the square of the blade speed, as seen in equation (10)(46) from [46] .

$$\psi = \frac{\Delta h_0}{U^2} \tag{46}$$

Where Δh_0 is the stagnation enthalpy change, and U is the blade speed. In an adiabatic machine, the stagnation enthalpy change is equal to the specific work, which then makes the stage loading be equal to the ratio of the change in fluid tangential velocity to the blade speed, as in equation (47) from [46] .

$$\psi = \frac{\Delta C_\theta}{U} \tag{47}$$

Where ΔC_θ is the ratio of the change in fluid tangential velocity. This means that the larger the stage loading coefficient, the larger amount of work is being done or used by a stage. An increase in stage loading coefficient will also produce a decrease in efficiency [64]. These two coefficients are important for this work because the combination of both can describe the performance of a single stage of a machine, and provide data for the simulation.